HYDROUS, LOW-CARBON MELTING OF GARNET PERIDOTITE

By

J. Brian Balta

Paul D. Asimow

Jed L. Mosenfelder

ABSTRACT

The presence of volatile species in Earth's upper mantle drives the formation of low-degree melts at pressures and temperatures where volatile-free mantle rocks would be subsolidus. The two most abundant volatile species, given the oxidation state of the Earth's upper mantle, are carbon dioxide and water. Understanding the influence of these species, separately and together, on melting processes requires well-controlled data on pure volatile systems as well as mixed-volatile experiments at the conditions of interest where these species have the most influence. We present experimental melting results from 3 GPa and 1375°C on hydrous systems with controlled water contents and rigorously minimized carbon contamination in order to analyze the effect of water on the melting of fertile peridotite KLB-1 in the garnet field. Compared to anhydrous experiments at this pressure, the addition of water to the peridotite produces a melt with an increased SiO_2 content relative to MgO and FeO. This effect is tantamount to an increase in the stability of olivine at the solidus relative to the other crystalline phases. There is also a substantial change in the composition of clinopyroxene in equilibrium with the melt; the clinopyroxene field contracts when water is added to the system, producing clinopyroxenes with higher CaO than typically found at these pressures. The contraction of the clinopyroxene field decreases the bulk partition coefficients of TiO_2 and Na_2O, which are less compatible in a hydrous system than an anhydrous system. We present an analysis of the remaining oxides and their behavior during hydrous melting, and compare our liquid composition to anhydrous experiments and modeled liquid compositions at similar pressures. The contraction of the clinopyroxene field during hydrous melting has important implications for melting of the mantle, including possibly

decreasing the bulk partition coefficient for water during melting and pushing the initiation of hydrous melting deeper into the garnet field.

1. INTRODUCTION

Water plays a fundamental role in the melting of Earth's mantle. Water strongly interacts with other components in non-ideal silicate melt solutions and therefore has direct effects on melt chemistry in equilibrium with residual solids. Furthermore, the presence of a volatile species, such as water, in upwelling mantle will allow a source rock to melt at higher pressures and lower temperatures than the same rock would if it were volatile-free, implying an indirect effect due to melting under different conditions and in the presence of different mineral assemblages and compositions. The direct and indirect effects together can significantly modify the composition of liquids generated in the mantle, and understanding the effects of water on the melting of the Earth's mantle therefore requires experiments on natural compositions (or close analogs) across the substantial range of temperatures, pressures, and compositions accessible to modern melting regimes.

Pioneering early work on hydrous melting of mantle-like compositions was conducted by Kushiro and co-workers, on simplified systems such as enstatite-H_2O (Kushiro et al., 1968), forsterite-enstatite-diopside-H_2O (Kushiro, 1969), and forsterite-diopsite-silica-H_2O (Kushiro, 1972). One important result of these simplified melting experiments is that the presence of dissolved water in a silicate melt in equilibrium with solids tends to drive the melt to higher silica contents. This is explained by the reaction between water and bridging oxygens in the tetrahedral silicate network, which depolymerizes the liquid and lowers the activity coefficient of silica (Mysen et al., 1980).

Moving past simple systems, a full accounting for the effect of water on the melting column must involve hydrous experiments on more complex systems, including

those without a free vapor phase where the activity of water is not fixed (as occurs in the mantle). Liu et al. (2006) produced experiments on hydrous liquid compositions in equilibrium with a simplified spinel lherzolite at 1.2 GPa pressure. Gaetani and Grove (1998) produced experiments on hydrous basaltic liquids in equilibrium with synthetic lherzolite and harzburgite lithologies at pressures from 1.2 to 2 GPa. Falloon and Danyushevsky (2000) and Parman and Grove (2004) also produced hydrous melts in equilibrium with harzburgite lithologies from 1.5 to 2.5 and 1.5 to 2.2 GPa, respectively.

While these experiments provide valuable information about the effect of water on melting, there are several differences between them and the style of hydrous melting likely to occur under mid-ocean ridges. First, under a mid-ocean ridge, water is expected to flux a low-degree melt at greater depths than are sampled by these experiments (Asimow and Langmuir, 2003) if the peridotite contains a few hundred ppm water by weight. These depths are typically expected to be in the garnet field (Asimow et al., 2004), and thus the solid mineralogy and likely the partitioning of a number of elements will be significantly different from that measured at lower pressures. Second, experiments conducted on analogue systems or in equilibrium with harzburgitic lithologies may also show compositions and partitioning significantly different from those in equilibrium with more fertile lherzolites. As hydrous melting is likely to produce only low degree melts, it is unlikely that their production would be able to deplete the solid residue enough to produce a harzburgite; higher degrees of melting at lower pressures would be required (e.g., Asimow, 1999; Kelemen et al., 1992). Finally, as noted by Liu et al. (2006), a common concern with hydrous melting experiments at any condition has been infiltration of carbon into experimental charges. As carbonate and

water can have a strong mutual interaction in a silicate melt phase, the presence of variable amounts of carbon entering a hydrous melt will affect the activity of water and potentially that of other reactive species in the liquid.

The production of melt within the garnet field under mid-ocean ridges in particular has been a longstanding issue. Trace element and isotopic characteristics of mid-ocean ridge basalt (MORB) have been interpreted to suggest that garnet is necessary as a residual phase in the melting zone (e.g., Salters and Hart, 1989; Shen and Forsyth 1995). However, this constraint is at odds with a number of other indicators which suggest that high temperatures and very high degrees of melting would be required to melt peridotite in the garnet field (Iwamori et al., 1995; Robinson and Wood, 1998), and measurements that suggest that the garnet signature is strongest in MORB representing lower total degrees of melting. Other solutions have been proposed to resolve this controversy, such as melting of distinct pyroxenites in the MORB source (Hirschmann and Stolper, 1996), elevated pressures of melting (Shen and Forsyth, 1995), or increased compatibility of rare earth elements in aluminous clinopyroxene (cpx) at high pressures (Blundy et al., 1998). Each of these proposed explanations for the garnet signature has potential complications. Pertermann and Hirschmann (2003b) examined experimental melting of pyroxenite bodies and found that they could not make up more than 2% of the MORB source region based on the differences in chemistry. The Shen and Forsyth model requires melting to stop at depths much greater than would be expected by melting models (e.g., Asimow et al., 1999), implies a correlation between crustal thickness and spreading rate which is not observed (White et al., 1992), and is inconsistent with other aspects of the major element chemistry (Kinzler, 1997). The partition coefficients (D =

concentration of species in solid/concentration of species in liquid) of Blundy et al. (1998) differ from those of other authors (e.g., Salters and Longhi, 1999) and require highly aluminous cpx that may not exist under certain circumstances (see below). As hydrous melting likely takes place in the garnet field and is expected to produce low degree melts, experiments on the chemistry of hydrous melting under typical mid-ocean ridge conditions may provide an alternative explanation for the garnet signature, and therefore investigation of melting under these conditions is necessary.

We have designed and conducted experiments with these issues in mind to illustrate the effects of limited quantities of water on the melting of fertile peridotite under low-carbon, garnet facies conditions. These experiments show first that the effect of water on the overall liquid composition is similar to that found by Gaetani and Grove (1998) on carbon-containing, lower pressure samples; the presence of water serves to decrease the ratio of (MgO + FeO)/SiO_2 and thus increases the SiO_2 content of the liquid if considered on a volatile-free basis. Second, we show that the presence of carbon, even at low concentrations, interacts with water in the liquid and may serve to counteract some of the effect of the presence of water. Third, we find that the interaction of hydrous melts with the fertile peridotite mineralogy has significant and unexpected effects on the modal abundance and composition of cpx during melting, and these effects are potentially very important for the partitioning of a large number of components of silicate melts. One specific consequence of the presence of garnet on the minor element makeup of silicate melts is detailed in Chapter 3 of this thesis.

2. METHODS

2.1 General approach

Producing equilibrium, low-degree melts has historically been a difficult problem for experimental petrology, as it is much easier to sample and analyze high-degree melts. Two general categories of methods have been explored that should be noted here: extraction methods and so-called sandwich methods. A number of authors have employed techniques based on the maintenance of open pore space or highly wetting surfaces towards which low-degree melts can segregate during experiments. Kushiro and Hirose (1992), Johnson and Kushiro (1992), Hirose and Kushiro (1993), Baker and Stolper (1994), and Baker et al. (1995) employed a diamond-aggregate technique, where pore space between diamond crystals was used to trap the initial melts extracted during melting. The intent of these experiments is for the rapidly extracted melt to diffusively equilibrate with interstitial melt in the solid pile and then to form an unmodified glass upon quenching because of its distance from nucleation sites for quench crystals. Later extraction techniques include crimped capsule or foil layers (Holloway and Kawamoto, 1997) or vitreous carbon spheres (Schwab and Johnston, 2001, Wasylenki et al., 2003, and Pertermann and Hirschmann, 2003a). For our experiments, the diamond aggregate technique would be inappropriate, as the presence of diamond or vitreous carbon would provide an immediate potential source of carbon if there were any reaction with oxygen in the sample, and vitreous carbon spheres are known to take up water on their own (Wasylenki et al., 2003). The presence of carbon-rich phases would also make accurate determinations of dissolved carbon contents difficult (Pertermann and Hirschmann, 2003a).

"Sandwich" experiments, as a general class, attempt to produce large, analyzable pools of low-degree melts that escape quench modification by reacting a melt of a

composition close to the predicted low-degree melt composition with solids until the liquid becomes multiply-saturated with the solids (Stolper, 1980, Takahashi and Kushiro 1983). Several ideas have been proposed to attempt to improve upon this technique. One difficulty is that the solid compositions tend to change as they react with the liquids, producing solids and liquids that are in equilibrium with each other, but which are not necessarily representative of the mantle. Wallace and Green (1988) and Robinson et al. (1998) proposed one solution: adding an iterative procedure, where each successive liquid is synthesized based on the composition measured in the previous experiment until the liquid and solid compositions no longer evolve during the run. This improves on the multiple-saturation technique by making the solid compositions more representative of the mantle. But, as our experiments will demonstrate, the high variance of natural peridotite equilibria imply non-uniqueness, namely that a range of solid and liquid compositions can be in equilibrium at the same conditions, all of which may satisfy a mass balance constraint and thus appear to be plausible equilibrium states of a given source composition. Furthermore, in the case of highly compatible or highly incompatible elements, it is possible that the liquid and solid compositions can be trapped in metastable local minima or in situations where many, many iterations are required to approach equilibrium. Hirschmann and Dasgupta (2006) proposed an approach to converge on the liquid composition at the solidus: measuring the solid/melt partition coefficients and calculating the next iterative liquid using the batch melting equation evaluated in the limit of zero melt fraction. This technique also has potential complications. First, highly-incompatible or highly-compatible elements may have partition coefficients that cannot be accurately measured due to low concentration in one phase. Second, calculating the

bulk partition coefficients requires accurate knowledge of the modal abundance of the solid phases, which may be difficult to estimate. Finally, this technique does not guarantee that the oxides will sum to 100% after its application, and therefore requires a choice to either exclude a closure component from the calculation or to renormalize the calculated solidus liquid composition, neither of which is an optimal approach.

For our experiments, we use a hybrid of the regular and modified iterative sandwich techniques. We set up the experiments in the conventional iterative sandwich format, reacting a hydrous liquid with solid garnet peridotite. At each step, we measure mineral/melt partition coefficients, calculate bulk partition coefficients, and use the modified iterative sandwich technique to calculate the concentrations of most of the oxides in the next candidate liquid. For very incompatible or very compatible elements and for elements such as SiO_2, where the forecasting method is unstable or compromised by closure, we will simply use the conventional sandwich technique and adopt the measured concentration in the melt as the concentration for the next candidate liquid. We use modal abundances calculated by least-squares solution of the mass balance constraint whereby the bulk peridotite composition must be a linear combination of the measured mineral compositions. We also consider the effect that shifts in the modal abundance of the solid phases would have on the bulk partition coefficients to estimate a reasonable range of possible natural compositions that could represent solidus melt compositions.

Assessing convergence of the iterative process is a difficult task, because the Gibbs phase rule suggests that the liquid in equilibrium with three solid phases at fixed temperature and pressure will still have multiple degrees of freedom in a natural system of >10 components, including the volatiles and the minor elements. Furthermore, the

partitioning of several elements may be determined by the particular liquid composition, especially if they interact strongly with the volatiles. Our approach is therefore to synthesize a liquid that is within the range of compositions that will be multiply saturated with the KLB-1 assemblage under these pressure and temperature conditions. Then, we will perform repeat experiments varying parameters such as the ratio of solid to liquid and the total water content to define the range of accessible liquid compositions and to attempt to constrain how the liquid composition changes with the parameters that we can adjust.

2.1.1 Solid preparation

A major concern for these experiments was the initial state of the solids added during each run. The equilibrium we want to observe is hydrous liquid with fertile garnet peridotite. Most of the commonly available natural fertile peridotites, however, are spinel or plagioclase peridotites due to reaction at low pressures during their ascent. If a spinel peridotite were mixed with a hydrous liquid under pressures where garnet is the stable aluminous phase, the sample could easily move away from the true equilibrium due to multiple ongoing reactions. For example, the melt might rapidly equilibrate with a slowly evolving population of pyroxenes as their modes and composition change due to the spinel to garnet reaction. It was therefore judged to be important to begin these experiments with a peridotite that was already stably equilibrated within the garnet field. This step will also be useful in providing a peridotite produced under the same pressure and similar temperature to our melting experiments for comparison of solid compositions.

To produce this peridotite, we took a sample of natural KLB-1 peridotite powder of variable grain size (kindly supplied by C. Herzberg, from the same powder as the

original KLB-1 of E. Takahashi) and ground it along with less than 1% by weight of a magnesian garnet from Arizona (supplied by G.R. Rossman, composition given in table 1). This garnet was added to give seed grains, reducing the needed reaction time by avoiding nucleation problems. The mixture was ground for several hours in an alumina mortar and pestle to reduce the maximum grain size from ~100 μm to ~1 μm or below. This grain size was required to allow for sub-solidus recrystallization on the timescales of these experiments. The powder was dried and loaded into a combined molybdenum/gold/palladium/iron capsule. The capsule was prepared by submersing a 3 mm outer diameter (o.d.) Au_{75}/Pd_{25} capsule in Kilauea 1919 basalt at 1190 °C for 48 hours under a controlled H_2-CO_2 gas stream with an fO_2 set at 1.6 log units below the QFM buffer, following the technique outlined in Chapter 4. This produced a capsule with ~4% dissolved Fe. The presence of Fe tended to make the capsule more brittle and likely to tear when compressed, so this capsule was hammered into a molybdenum sheath to prevent tearing. The sheath was made by drilling a 3 mm. hole into a 4 mm o.d. molybdenum rod, with a 1 mm thick lid cut from the same stock and used to cover the capsule during the high-pressure experiment. The powder was packed into the capsule, and the full capsule was heated to 1000 °C under a H_2-CO_2 gas stream with an fO_2 set 2 log units below the QFM buffer, within the range of predicted mantle values. This step was necessary to devolatilize the peridotite, and the gas stream was used to prevent oxidation of the sample during heating. The capsule was then removed from the furnace and kept at 300 °C until the gold-palladium capsule was welded shut. The molybdenum lid was placed on top of the capsule loosely during loading and welded itself to the remainder of the capsule upon compression.

All of our experiments were conducted at a nominal pressure of 3 GPa in a ½" piston-cylinder device. The cell was composed of an outer sheath of calcium fluoride as pressure medium, a straight-walled graphite heating element, and crushable MgO spacers to center the capsule in the hot spot. Temperature was monitored during the run using a $W_5Re_{95}/W_{26}Re_{74}$ thermocouple (type C), with no pressure correction on the E.M.F., and recorded temperature fluctuations were typically 2 °C or less. Experiments were first placed at pressure and allowed to sit for a period of at least an hour to allow for compaction before heating; this technique seems to help provide a seal against volatile loss or gain during heating of the run. No correction was applied to the pressure to account for friction. Previous calibration work on this press suggests that the nominal 3 GPa pressure may require a negative correction of up to 0.2 GPa (Mosenfelder et al., 2006). However, the calibration work was done at much lower temperatures and this misfit may decrease with increased temperature due to decreasing friction. Consequently, we estimate that all experiments here were performed at an identical pressure in the range of 2.8-3.0 GPa, pending refinement by further calibration work. The recrystallization runs were held at a measured temperature of 1350 °C and (nominally) 3 GPa for a period of at least 336 hours. The experimental temperature should be below the dry solidus of KLB-1 (Herzberg et al., 2000) and samples did not melt unless the capsule failed. The run times were long enough to homogenize the sample to the level measured by electron microprobe in all major and measured trace elements (Figure 1) except for NiO, which declines significantly near the edge of the sample due to Ni loss to the capsule. Temperature gradients within the capsule are possible and have not been calibrated, but

the homogeneity of the final samples suggests that they are limited to <20°C in both the sub-solidus and the melting experiments.

2.1.2. Liquid preparation

The hydrous liquid in these experiments was synthesized from laboratory grade oxides and carbonates. The initial seed liquid for the iteration was the calculated solidus liquid with 1 wt. % H_2O from KLB-1 peridotite at 3 GPa according to the pHMELTS algorithm (Smith and Asimow, 2005). Further liquids were synthesized based on the resulting liquid compositions. The mix was initially made with a deficit of Al_2O_3 since H_2O would be later added in the form of gibbsite ($Al(OH)_3$). Oxides and carbonate reagents were first dried individually, mixed by weight, ground under ethanol for >8 hours, and step-heated to 800 °C in air to decarbonate the mixture. The mixture was then placed at 1000 °C for ~12 hours at fO_2 10^{-13} bars to convert most of the iron into Fe^{2+}. The mixture was then heated in a platinum crucible above 1450°C in an H_2-CO_2 gas stream with fO_2 2 log units below the QFM buffer, for 1 hour. The crucible was previously iron-preconditioned using the technique of Kessel et al. (2001) to avoid iron-loss to it. Na_2O is expected to be the most volatile element during this procedure (e.g., Tsuchiyama et al., 1981) and no significant Na_2O loss was observed during sample preparation. The liquid was quenched to a glass by immersing the crucible in water. The glass was then broken apart and re-ground for 4 hours along with powdered gibbsite as a water source, with the amount calculated to make up for the missing Al_2O_3 and to give several wt. % H_2O. Gibbsite was used because we were able to verify by mass spectrometry that the gibbsite was carbon-free; other water-containing minerals, such as

brucite, were found to be carbon-contaminated and could not be used for controlled-carbon experiments.

2.1.3. Capsule design

Our capsule design was key to meeting our experimental goals of maintaining hydrous samples while avoiding carbon infiltration or other changes in parameters such as fO_2 that could affect the equilibrium liquid composition. We adapted the double-capsule design proposed by Kägi et al. (2005), which was originally used as a means of controlling fO_2 in hydrous experiments. The capsule was constructed by loading a 1.6 mm. o.d. iron-preconditioned $Au_{75}Pd_{25}$ inner capsule with a mixture of roughly equal proportions of the recrystallized garnet peridotite (see above) and a powdered hydrous glass (see above). After welding (see below), this inner capsule was loaded along with more of the same powdered hydrous glass and extra liquid water into an outer capsule made from a larger iron-preconditioned 3.8 mm o.d. Pt tube (Figure 2). The extra water was loaded by microsyringe because the diffusion of hydrogen through platinum is faster than through $Au_{75}Pd_{25}$ (Chou, 1986). Both the outer and inner capsule were arc welded shut with the cold end immersed in a bath of liquid nitrogen to avoid excessive dehydration during welding, which was a major issue for the smaller capsules. The inner capsule was Fe-preconditioned using the calibration of Chapter 4 of this thesis, and the outer capsule was Fe-preconditioned using the calibration of Kessel et al. (2001). The outer capsule contained up to 20 times more glass than the inner capsule and was intended to serve as a large reservoir to slow the diffusion of carbon into the sample from the exterior. The likely source of carbon contamination is the graphite heating element

used in the cell. In addition to buffering the water content and oxygen fugacity, this technique was found to effectively slow diffusion of carbon into the inner capsule.

2.1.4. Melting experiments

Melting experiments were run using the same piston-cylinder protocol as described above for the subsolidus recrystallization experiments except for temperature and time. Melting was conducted at 1375 °C for periods from 6 to 20 hours. Quenching hydrous basaltic glasses from 3GPa has historically been a challenge. Our experiments were quenched by shutting off the power; this achieved quench from the run temperature to < 200 °C in under 10 seconds. Coincident with the time of quenching, we dropped the pressure by releasing the oil pressure in the master ram cylinder. This technique was similar to that employed by Putirka et al. **(**1996), but we did not drop the pressure as aggressively prior to quenching because the melting point of $Au_{75}Pd_{25}$ alloys is close to the experimental temperature and too large a pressure drop could have caused the capsules to cross their melting point by decompression. Obvious vesiculation on quench was not observed.

2.2. Analytical techniques

Capsules were sectioned using a K.D. Unipress type WS-22 wire saw, with a cut down the centerline to hopefully cross the inner capsule. One half of the capsule was mounted in and vacuum-impregnated with epoxy, polished using alumina and diamond grits, and carbon coated for analysis by electron microprobe and scanning electron microscope. Quantitative analyses were conducted using the JEOL JXA-8200 electron microprobe at the California Institute of Technology in wavelength dispersive mode. Liquid compositions were measured using a current of 10 nA and a spot size of 15-20

μm, with 20 seconds counted on-peak and 10 seconds counted off-peak. Sodium and potassium were counted first to minimize loss of volatile elements. Lower current analyses were also performed to confirm that sodium and potassium were not being lost. Solids were analyzed using a focused beam, a current of 30-40 nA, and identical counting times.

Volatile contents in the glasses were measured using a Nicolet Magna 860 FTIR spectrometer coupled to a Spectra-Tech Continuum microscope. Spectra were obtained on doubly-polished sections of the experiments from 1000 to 6000 cm^{-1} using unpolarized light, a KBr beamsplitter, and an MCT-A detector. Sample thickness and flatness were checked using a digital micrometer close to the analyzed spots, and wedging was typically limited to a few micrometers. We used rectangular apertures greater than 30 μm in the short direction and attempted to avoid contamination by solid phases, cracks, and edges. Multiple spots were checked on several samples to establish homogeneity of volatile contents (typically better than 10% across single runs). Water contents were calculated from absorbances based on the composition-dependent calibration of Ohlhorst et al. (2001) and electron probe analyses of the major-element glass composition. Slight extrapolation was required, as the lowest SiO_2 content used in the calibration was 50%, while our liquids have slightly lower total SiO_2. Carbonate contents were calculated using the calibration of Fine and Stolper (1986). Glass densities were calculated using the iterative technique of Aubaud et al. (2007), although their calibration does not include carbonate. Linear background corrections and a manual subtraction procedure were used, potentially giving small additional errors on each analysis.

Overall, we estimate the relative error on the volatile content calculations to be ~10% based on the repeat analyses of individual samples (1σ), which is sufficient for the purposes of this study. The largest sources of error are measurement of the sample thickness at the site of analysis and the exact absorbance calibration. Typically, for the measured water contents, the absolute error is about ± 0.5% H_2O. This error is of similar magnitude to the error on the calibration for the absorbance peaks used. Reduced errors on similar analyses are likely possible in the future, but would require a more detailed understanding of the relationship between the multiple peaks near 4500 cm^{-1} (see below) and the total water content, and calibration of absorption coefficients across a wider range of silicate liquid compositions including picritic basalts and basalts with variable amounts of carbonate.

To confirm the calibration, we analyzed several samples at different thicknesses, allowing us to calculate water contents based on the OH^- vibration peak at ~3600 cm^{-1} and by a combination of the H_2O and OH^- vibration peaks at ~5200 and ~4500 cm^{-1}. The errors on the 3600 cm^{-1} peak are estimated to be much smaller and do not require significant recalibration for the liquid composition; for this peak, we used the absorption coefficient of Dixon et al. (1995). For the overtone peaks, sample thicknesses of >100 μm were commonly used, while sample thicknesses <50 μm were necessary to bring the 3600 cm^{-1} peak on scale. These repeat measurements at different thicknesses and typically on different spots produced total water contents on individual samples that were within 2% of each other, significantly less than the estimated analytical error.

2.2.1. MELTS Calculations:

For comparison with our experimental liquid composition, we produced several calculated hydrous, low-degree silicate melt compositions using pHMELTS (Smith and Asimow, 2005). The calculations were done two ways (a sort of numerical reversal experiment), to ensure that the algorithm was not being caught in local minima. We used the solid KLB-1 composition, edited to improve the calculation by avoiding elements that the algorithm does not treat well (no potassium or manganese) and calculated the equilibrium melt composition at 3GPa and 1375°C, beginning with excess water. We then decreased the available water content towards zero until the melt composition did not change significantly at each step. Next we started the calculation subsolidus and found the initial melt composition during heating, varying the water content until the solidus was reached at 1375°C. These two calculations produced similar liquid compositions, although they required slightly different bulk water contents.

3. RESULTS

3.1. Recrystallization experiments

We have reproduced several nearly-identical sub-solidus peridotites from our KLB-1 starting mix showing no obvious evidence for zonation other than in NiO (Figure 1), which can be interpreted as evidence for close approach to equilibrium (Parman and Grove, 2004). The texture appeared to show additional evidence of equilibrium, with subhedral to euhedral grain shapes and developed triple grain junctions. The peridotites consisted of mixtures of olivine, cpx, and garnet. No orthopyroxene (opx) was observed in any experiment, as was predicted for the KLB-1 composition by Longhi (2002). Final mineral grain sizes were between 5 and 20 μm for all minerals. Average mineral compositions are reported in Table 1. Olivine Mg#'s (= 100 * molar MgO/[MgO+FeO])

averaged 89.8, consistent with fertile upper mantle and suggesting limited iron loss to the capsule. Using the bulk KLB-1 composition given by Davis et al. (2009) and our measured mineral compositions, we estimated modal abundances by least-squares mass balance; there was typically a slight residual on CaO (which could reflect contamination of the sample by natural caliche). Mineral compositions and calculated modal abundances are given in Table 1.

3.2. Hydrous melting experiments.

All reported experiments produced a hydrous, low-carbon basaltic glass in equilibrium with solid garnet, cpx, and olivine (Figure 3). Opx was only observed in the initial experimental step which started with a higher silica liquid composition; none was observed in equilibrium with the final estimated solidus liquid composition, consistent with the lack of opx in the solid KLB-1. A single opx composition from an early iteration is reported in Table 1 for comparison to opx measured by others in anhydrous experiments. The double-capsule technique was successful at limiting carbon diffusion when the inner capsule remained intact. A number of times, however, the inner capsule was either partially dehydrated or failed during the run and contained limited hydrous silicate glass that was typically highly quench-modified due to the abundance of surfaces for nucleation. However, in such experiments, the volume of the outer capsule was often still sufficient to produce a low-carbon, hydrous, silicate glass that had reacted and equilibrated with the solid assemblage; in these runs the large volume was sufficient to accomplish the major experimental goals of hydrated liquids with limited carbon contamination. Hence, they were sometimes used as iteration steps to predict subsequent

liquid compositions. Measured carbon contents were a factor of 5-10 lower than those reported by Gaetani and Grove (1998) (Figure 4).

Experiments contained large amounts of measurable silicate glass (Figure 3), in pools up to ~500 μm in diameter. Basalts wetted most crystal surfaces, giving opportunity for full reaction of the liquid with the solids. Solids always sank to the bottom of each capsule regardless of loading configuration. Samples did show substantial modification on quench. Virtually all solid grains showed an iron-rich quench rim 1-3 μm thick that was avoided during probe analysis except in a few samples where the cpx grains were too small to analyze without contamination; no other zonation was commonly observed in the crystals. Interstitial liquid occasionally formed quench needles, and was always depleted in MgO and FeO compared to the large melt pool. Elongate quench needles were common at the boundary between solids and liquids. The boundary between the capsule walls and the liquid pool commonly showed quench crystallization of 10 to 100 μm of pargasitic amphibole of a composition close to the unmodified glass. In all cases, these quench features were avoided for analyses. Large pools of homogeneous glass were still available despite these quench features. In some samples, 100 nm-scale phases were observed visually within the glass pools, presumably also occurring on quench. However, these phases were much smaller than the activation volume of the electron probe or the wavelength of the infrared radiation, and no obvious change was observed in compositions between areas with and without those phases, although the quench phases may have slightly affected the Fe/Mg ratio and thus the calculated K_D for some experiments. Still, the assumption of homogeneous glass is very likely adequate even in those cases.

Establishment of equilibrium in this variety of experiment is difficult, as an appropriate reversal experiment test has not been devised. Several techniques suggest that these experiments either achieved liquid/solid equilibrium or were very close. First, measured values of the olivine liquid K_D parameter were between 0.32 and 0.40 and most consistently near 0.35-0.36. The calibration of Toplis (2005) predicts a K_D value of ~0.36 at these liquid compositions, with K_D increasing as H_2O content decreases. Our measured K_D values are consistent with the K_D values reported by Gaetani and Grove (1998) on their hydrous experiments from lower temperatures and pressures, and are generally within the range deemed acceptable by Toplis (2005). Two samples have high K_D values (0.38 and 0.40), potentially reflecting either disequilibrium between the liquid and the solids due to Fe loss to the capsules or slight changes in the Fe-Mg distribution on quench. However, the overall difference in liquid composition appears small and confined to the Fe-Mg system, which will be treated together, and therefore the data for these experiments are still included here. These two samples would require a loss of less than 10% of the available Fe in the liquid to the capsule to be consistent with the other measured K_D values.

Iron contents were variable between successive experiments due to the initial condition of the liquid and the capsule. The initial guess composition was higher in Fe than the final composition, and therefore the initial capsules were prepared with higher Fe than necessary. For the initial experiments, the capsules buffered the iron content at a higher level than predicted; this produced olivines with Mg# 86-87 and liquids with lower MgO contents than would be expected in actual mantle liquids. Capsules were then resynthesized with less Fe to equilibrate with a lower-iron liquid composition; these

liquids equilibrated with Mg# 88-90 olivine, close to the expected mantle value. Measured liquid and solid compositions are given in Table 2.

Additional evidence that these samples either represent equilibrium assemblages or at least close approaches to equilibrium comes from a number of sources. Typically, Fe-Mg zoning, which would be commonly expected in the case of significant Fe loss or gain, is easily seen in electron microprobe transects across single grains or visually, using back-scattered electron imagery (BSE). In our experiments, zoning is typically only barely visible in BSE imaging (Figure 3), and measurements of solid compositions from cores and rims of grains are typically indistinguishable if obvious quench features are avoided. A lack of clear zoning has been taken previously as evidence for close approach to equilibrium (Parman and Grove, 2004). If these experiments were far from equilibrium, significant zoning would be expected as the solid compositions shift substantially during the run (see below). Additionally, experiments were run for different durations from 6-20 hours, and there was no correlation between zoning and experiment duration, suggesting that much of the reaction is rapid relative to the timescales of the experiment. Finally, as nickel was found to be compatible in our capsules, measuring grains with significant nickel contents would suggest a lack of equilibrium, and this was not observed at the level of the errors on the electron microprobe analyses (Table 2). While these experimental timescales are short compared to those run by others (e.g., Parman and Grove, 2004, Walter, 1998) the small grain sizes and high water contents likely allowed fast reaction between the solid and liquid assemblages, allowing for a close approach to equilibrium on the timescale of these experiments.

Volatile compositions were measured on the glasses via FTIR. Measured volatile compositions combined with electron probe totals typically gave totals that were 98% or better. Mismatch decreased in the samples with lower measured water contents. Typical water-containing glass spectra are displayed in Figure 5. Significant and unexpected structure was observed in the IR spectra. We report the first analyses of water-containing glasses that show the 4500 cm^{-1} peak split into multiple peaks, typically a triplet, rather than a single peak. In more evolved basaltic liquids, a single peak near 4500 cm^{-1} is common, and a small shoulder is occasionally observed (Sally Newman, personal communication, 2009). In our experiments, observation of multiple peaks near 4500 cm^{-1} was common. In many minerals, this region of the IR spectrum shows complexity due to bonding between the OH^- groups and other structural elements in the mineral (e.g., Bishop et al., 2002). Our composition differs from previously analyzed basalts in several ways that could be related to the peak-splitting. Typical basalts that have been measured before were often lower in total MgO than these basalts (Dixon et al., 1995); our liquids have much higher total MgO and FeO than fractionated MORB, for example. It is also possible that the strong interaction of carbonate and water at high pressures could produce changes in the IR spectra. We hypothesize that the normal 4500 cm^{-1} peak splits into multiple peaks in our experiments because of interactions between the Si-O-H groups and other components in the melt. Specifically, our experiments have much higher MgO contents and possibly CO_3^{2-} contents than most natural erupted basalts due to the fractional crystallization and degassing processes that affect natural liquids prior to eruption, and these interactions may be the cause of these additional peaks.

Interaction was possibly observed between the water and carbonate groups in the liquid. At low carbon contents, the 4500 cm^{-1} peak was a similar thickness-normalized height in multiple experiments. At higher carbonate concentrations, the 4500 cm^{-1} peak was observed to increase in size (Figure 6). This interaction suggests that the carbonate is serving to create additional bridging oxygens that can be separated by reaction with water to give additional hydroxyl groups, and this carbonate interaction is a potential explanation for the splitting of the IR peaks. The lowest water-content sample, R380, falls off this trend. This sample could fall away from the trend if it is not fully saturated in OH^- because of its lower water content. Dixon and Stolper (1995) showed that it took significant total water contents, typically ~4% H_2O, to fully saturate a basaltic liquid in OH^-. The remaining liquids have higher water contents, may thus be much closer to saturated in OH^-, and may better demonstrate the interaction between the water and carbonate species.

4. DISCUSSION

Previous experimental and theoretical work allows for the evaluation of our liquid and solid compositions via comparison with anhydrous liquids from these pressures, hydrous liquids from lower pressures, and calculated liquid compositions. Anhydrous experiments from 3-7 GPa on fertile peridotites were conducted by Walter (1998) and have served as the basis for analysis of melting at these pressures by a number of workers (e.g., Humayun et al., 2004; Herzberg, 2006). Longhi (2002) produced anhydrous melting experiments from 2.4-3.4 GPa with similar compositions to those reported by Walter (1998), used those experiments as the basis for creating the empirical BATCH calculator, and applied the calculation to anhydrous peridotite melting under similar conditions.

Gaetani and Grove (1998) produced hydrous, carbon-containing liquids at lower pressures, from 1.2 to 2 GPa. All these experiments and the calculated liquid composition from pHMELTS will be used to place our results in context. Following the approach of Gaetani and Grove (1998), we will analyze these liquids both on a renormalized volatile-free basis, to allow for direct comparison with volatile-free melting experiments, and on a hydrous basis to attempt to better constrain the underlying thermodynamics, and partitioning. An average composition, based on our experiments, that should be in equilibrium with Mg#~89 olivine is given in Table 3, presented both on a hydrous, low-carbon basis and on a volatile-free basis, normalized to 100% total. Also given are liquids from the closest temperature and pressure conditions available from the other four studies mentioned above. The pHMELTS algorithm calculates a liquid that is vastly over-enriched in Na_2O, as discussed later. This necessitates care when using individual oxide compositions from those calculations to make inferences; ratios of one oxide to another and normative mineral components will be considered as, in many cases, these quantities are more robust (except those involving Na_2O). Volatile-free liquid compositions are displayed graphically in Figure 7 for comparison.

4.1. MgO, FeO, SiO_2

The effect of the addition of H_2O on the MgO + FeO and SiO_2 contents of silicate melts has been a major source of controversy since it was originally proposed that direct hydrous melting of peridotite was a method of producing high-silica, andesitic melts from the mantle (e.g., Kushiro, 1972). In their peridotite melting experiments, Gaetani and Grove (1998) proposed that the major effect of the addition of water during melting was to move the liquid from olivine-normative to quartz-normative by increasing the SiO_2

content of the liquid when considered on an anhydrous basis, which led to a similar decrease in the (MgO + FeO)/SiO_2 ratio. When considering the hydrous components, however, those authors found that the SiO_2 content of the liquid actually decreased slightly with additional water. Based on a more simplified system, Liu et al. (2006) agreed that the MgO/SiO_2 ratio decreases in hydrous liquids, but noted that the SiO_2 content of the liquid did not appreciably change as H_2O was added. Therefore, the change in MgO/SiO_2 in their experiments was due entirely to the decreasing MgO content of the liquid with increasing water. While their system used only MgO, our liquids contain both MgO and FeO — both major components of olivine — and thus we will consider these oxides jointly. The pHMELTS algorithm calculates a hydrous liquid with a much lower SiO_2 content than our liquid and the highest (MgO + FeO)/SiO_2 ratio of any near-solidus liquid considered here.

Comparison of the results of our melting experiments with the anhydrous liquids from 3 GPa of Walter (1998) and Longhi (2002) shows that our experiments typically have less SiO_2 than either of the predicted liquid compositions when our results are considered on a hydrous basis (Figure 8). When renormalized to volatile-free conditions however, the SiO_2 content of our liquids becomes higher than the SiO_2 content of the anhydrous liquids. This result is consistent with the effect of water on peridotite melts observed at lower pressures by Gaetani and Grove (1998). However, our liquids show SiO_2 contents when considered either on hydrous or volatile-free bases that are similar to or higher than the liquids measured by Gaetani and Grove (1998) at lower pressure. This behavior is somewhat surprising, as their experiments typically contain opx, and the silica activity fixed by the opx-olivine equilibrium is known to shift to lower values with

increasing pressure. Our experiments lack opx, and so should lie at still lower SiO_2 activity than the opx-olivine buffer. Both higher pressure and opx-undersaturation suggest that our experiments must have lower SiO_2 activity than those of Gaetani and Grove (1998) and yet the SiO_2 content of our liquids is not lower. There are several possible explanations. Liu et al. (2006) noted that there was a correlation between increasing Na_2O in their liquids and increasing silica content. Our liquids do show higher Na_2O than the liquids considered by Gaetani and Grove (1998), which could have a corresponding effect on the silica activity coefficient and silica content. Liu et al. (2006) also noted that the presence of CO_2 can serve to counteract some of the effect of the addition of water to liquids. While Liu et al. (2006) did not note any significant change in SiO_2 due to the addition of water, our experiments and those of Gaetani and Grove (1998) both show increasing liquid SiO_2 contents with increasing water (Figure 8). The high carbon contents in the experiments of Gaetani and Grove (1998) could drive the liquid to lower SiO_2 values because of the interaction between CO_3^{2-} and the hydrous liquids. Another possibility involves the cpx composition and the effects of CaO in the pyroxene quadrilateral, which may destabilize opx in our runs in a way that is not obvious from the dynamics of the MgO-FeO-SiO_2 ternary (see below).

The MgO content of our liquid can be understood in a similar fashion, in particular when both the MgO and FeO content of the liquid are combined into normative olivine. As described above, the FeO content of our liquids is fixed by the composition of the capsule material containing it. In the higher FeO experiments, the MgO content of the liquid adjusted to a lower value by solid crystallization. When compared to the liquids of Walter (1998), Longhi (2002), and that calculated by pHMELTS, our hydrous liquids are

measurably lower in (MgO + FeO)/SiO_2 (Figure 8). Compared to the hydrous compositions from lower pressure, our experiments show higher MgO + FeO contents. This is likely due to the well-established increase of total liquid MgO + FeO in equilibrium with the solid lherzolite assemblage with increasing pressure and temperature (Longhi, 2002). Our experiments are at higher pressure and higher temperature than the hydrous experiments of Gaetani and Grove (1998) and thus have higher MgO + FeO contents, while the MgO + FeO contents are lower than those from the hotter, anhydrous experiments of Longhi (2002) and Walter (1998). Liu et al. (2006) showed that an increase in water content of a liquid was associated with a decrease in MgO content, similar to these experiments.

An alternative and equivalent description for this set of changes is that the addition of water to the liquid expands the stability field of solid olivine relative to the other phases present (Figure 9). Longhi (2002) showed that as the pressure increases on a solid peridotite assemblage, the melt in equilibrium with the full peridotite assemblage increases in olivine component. As the pressure and temperature of melting increases, the olivine liquidus field contracts and the liquid composition moves towards olivine on a phase diagram. The addition of water decreases the (MgO + FeO)/SiO_2 ratio, as shown earlier, and moves the liquid composition away from olivine (Figure 9). Adding water to a silicate liquid has the effect of depolymerizing the liquid; bridging oxygens are separated by the reaction of water that produces OH^- groups. This effect on the liquid qualitatively makes the liquid more “olivine-like”, in the sense that the olivine structure contains no bridging oxygen atoms and would be considered fully depolymerized. During crystallization of liquids at low pressure during cooling, the effect of water is well

established: increased water content causes additional crystallization of olivine relative to the other phases (e.g., Asimow et al., 2004). The addition of water at pressure during melting appears to have a similar effect. Although a rigorous explanation of these relationships would require detailed understanding of the relationship between liquid speciation and component activities, it is frequently true that, just as making a liquid compositionally more like some solid tends to move the liquid towards the liquidus field of that mineral, so making a liquid structurally more like olivine has a similar effect.

The liquid calculated by the pHMELTS algorithm misses the effect of water on the $(MgO + FeO)/SiO_2$ ratio by the largest amount. The program likely has only a limited knowledge of the effects of water on the phase relations at high pressure and was previously not calibrated with any knowledge of the effect of CO_3^{2-} on the melting relations, which could further obscure this trend in the calibration of that model. In addition, the effect of H_2O in that model may be overwhelmed by the effect of the large Na_2O content of the calculated liquid.

4.2. Al_2O_3

When considered on a volatile-free basis, the Al_2O_3 content of our liquid appears to be controlled by the presence of garnet in the equilibrium solids. While not all of the experiments of Walter (1998) contained garnet, and no single experiment at 3 GPa reported analyses of both garnet and liquid compositions, one can estimate a liquid composition in equilibrium with garnet at 3GPa by extrapolation from Walter's data. Our liquid has a similar renormalized Al_2O_3 content to that estimate. Compared to the experiments of Gaetani and Grove (1998), which were all at least partially within the spinel field or were much closer to the spinel to garnet transition, our liquid is

substantially lower in Al_2O_3 content than any of their liquids. This comparison suggests that the increasing stability of garnet with pressure causes a significant decrease in liquid Al_2O_3 content, while the presence of water may have little effect on the stability field of garnet at these conditions compared to the effects of temperature and pressure.

Longhi (2002) presented several calculations of liquid compositions using his BATCH program that show interesting behavior in Al_2O_3. The model recovers the high-melt fraction experimental result of Walter (1998) closely. The calculated liquid composition from a 1% melt of primitive upper mantle (PUM) had notably lower liquid Al_2O_3 than the higher melt fraction calculation. As our volatile-free aluminum contents are close to those of Walter (1998) this could suggest that our experiments are slightly higher-degree melts than hoped. However, since our experiments are saturated with garnet, the presence of this abundant, high-aluminum phase may impose a practical limit on liquid Al_2O_3 contents. An alternative explanation could be that the PUM composition used by Longhi (2002) is richer in opx than KLB-1. Longhi (2002) acknowledges that the BATCH program does not recover very well the compositions of the pyroxenes in the calibration experiments, in particular their Al_2O_3 contents. Our pyroxenes are also very different from the pyroxenes in anhydrous experiments due to the effect of water on the phase equilibria for cpx (see below). The lack of opx combined with the decreased concentration of Al_2O_3 in cpx may make Al_2O_3 slightly more incompatible even in the presence of garnet, and thus could push Al_2O_3 slightly higher even in low-degree melts.

The pHMELTS algorithm shows Al_2O_3 to be much more compatible relative to the other oxides than seen in our experiments. The model predicts a negative correlation between liquid Al_2O_3 contents and water contents during melting (Asimow et al., 2004),

which is not observed in these experiments. The algorithm appears to overestimate the stability of garnet during melting, including too little garnet in the melting reaction relative to the pyroxenes.

4.3 CaO

CaO is perhaps the most interesting oxide in our experiments, in that its behavior cannot be understood by a simple relationship between a constant solid and liquid composition. Consequently, varying CaO abundances was the main reason why the MISE procedure of Hirschmann and Dasgupta (2007) could not be applied fully to all phases.

At low pressures, a large miscibility gap exists between cpx and opx. As pressure increases on solid peridotite, the stability field of cpx expands significantly, and eventually the cpx field expands enough that opx is no longer stable in most common peridotites (Longhi and Bertka, 1996). In our sub-solidus equilibration experiments on a KLB-1 composition, this behavior is clearly seen. The peridotite begins as a mixture of olivine, opx, cpx, and spinel. The initial cpx was measured to contain ~19.5% CaO by weight (Davis et al., 2009). After recrystallization at 3 GPa, the spinel and opx have both reacted out, producing garnet and a cpx with a much lower CaO content, typically ~12%. This behavior is consistent with the compositions of the cpx grains measured in the anhydrous melting experiments discussed here. The CaO content of the cpx in the study of Walter (1998) decreased with increasing temperature or pressure, 10.65% at 3 GPa. Our peridotite was recrystallized at a temperature 150°C below the lowest temperature experiment from Walter (1998) and thus shows a slightly higher CaO content, but overall the behavior is very consistent. The cpx measured by Longhi (2002) show even lower CaO contents at similar pressures and temperatures. The cpx from our sub-solidus

experiments plot very close to the predicted edge of the 2.8 GPA cpx field from Longhi (2002) (Figure 10).

Gaetani and Grove (1998) conducted lower-pressure experiments that were both hydrous and anhydrous, and noted that there was a slight increase in the CaO content of their cpx in their hydrous experiments at 1.6 GPa. However, because the expansion in the cpx field occurs mostly at pressures higher than sampled by their experiments, the effect was minimal.

When the cpx in our recrystallized peridotites is exposed to a hydrous silicate melt, there is a significant shift in the equilibrium cpx composition. The cpx emerged from every hydrous experiment with ~17% CaO. Graphically, this composition plots well inside the anhydrous field boundary for cpx from these pressures, suggesting that there has been substantial contraction of the cpx field due to the presence of the hydrous melt (Figure 10). There is only slight variation in the pyroxene composition between successive runs, and these variations potentially correlate with the alkali and water contents of the liquid, although these relationships could be complicated by the presence of small amounts of carbonate. This change in solid composition violates one of the precepts for the iterative sandwich experiment, that the solid composition introduced at each step should be the same as the solid composition at the end of the experiment, and thus prevented completion of a full iterative sandwich procedure.

The change in the equilibrium cpx composition in hydrous samples has potentially significant implications for melting of variably enriched sources. The increasing CaO content of a cpx will have two competing effects on the bulk partitioning; CaO would be expected to be more compatible with this change, as the CaO content of

the solids has increased. However, this contraction in the cpx field could also have the effect of decreasing the modal abundance of cpx, perhaps by stabilizing opx to higher pressure. As experiments at higher pressure typically show a gradual decrease in the liquid CaO content (Walter, 1998), we believe that the contrary effect of re-contracting the cpx field will be to slightly increase the expected CaO content of the liquid in equilibrium with peridotite, but this will depend strongly on the overall bulk composition.

Compared to the other available experiments, this conclusion appears to be supported by our data. At all conditions, the liquids of Longhi (2002) are significantly lower in CaO content than our liquid. This is also true of our liquid compared to the calculated low-degree melt of PUM from the BATCH program. More useful than CaO concentration itself is the CaO/Al_2O_3 ratio, as Al_2O_3 shows little change once buffered by garnet, but may be useful as an indicator of degree of melting. The experiments of Longhi (2002) have significantly lower CaO/Al_2O_3 ratios than our experiments, again suggesting that CaO is more incompatible in the case of hydrous melting.

Compared to the 3 GPa experiments of Walter (1998), our liquid has a slightly lower CaO content. The CaO/Al_2O_3 ratio of our liquid is also lower than that of Walter (1998), although the difference is smaller. This potentially relates to the presence of opx in those experiments, which would make CaO more incompatible in the solids than in our experiments that are lacking opx.

The hydrous experiments of Gaetani and Grove (1998) show CaO contents that are slightly higher than our liquid. This is not unexpected, as the CaO content of a liquid in equilibrium with a full lherzolite assemblage should decrease with increasing pressure as discussed above. The cpx in our experiments has slightly lower total CaO than the

experiments of Gaetani and Grove, suggesting that the cpx composition field has expanded slightly, causing the change in liquid CaO content (Figure 10). Our liquid however is higher in CaO/Al_2O_3 than the liquids of Gaetani and Grove (1998) due to the lower Al_2O_3 in our experiments as discussed above.

Comparison with the pHMELTS model-calculated liquid perhaps best illustrates the effect of the contraction of the cpx field on the melt composition. The pHMELTS-calculated liquid has the lowest CaO content and lowest CaO/Al_2O_3 ratio of any liquid given here. Thus, the algorithm believes that under these conditions, CaO is substantially more compatible than actually seen in our experiments. The pHMELTS algorithm calculates a higher fraction of pyroxenes and garnet in the KLB-1 mix than we see at any step, and consequently it predicts CaO significantly more compatible than is seen in any of the available experiments.

It is more difficult to postulate a mechanism for this cpx behavior than it was for olivine, as the interaction of olivine with hydrous melts has been much more thoroughly studied. The pyroxene structure involves some sharing of oxygen atoms between silica tetrahedral, and so is more polymerized than olivine. Adding water to a silicate liquid therefore is qualitatively making the liquid less pyroxene-like and therefore should reduce the stability of cpx relative to the anhydrous case. One possible explanation is that the presence of water decreases the stability of cpx enough that high-Al_2O_3 cpx becomes particularly unstable and only a higher calcium cpx similar to those seen at lower pressures can remain stable. Alternatively, the chemistry could be viewed as water destabilizing the opx component in the solid. Longhi (2002) and others suggest that in anhydrous systems, opx should be a product of the melting reaction at 3 GPa. If the

presence of water instead moved opx back to being a reactant, the melting reaction could proceed by drawing the opx component out of the cpx and into the liquid. This mechanism could be illustrated qualitatively in Figure 10 by the motion of our measured liquid compositions away from olivine and the liquid composition from Longhi (2002) and towards opx with increasing water contents.

4.4. Na_2O

The Na_2O content of low-degree silicate melts from pressure has long been an open question due to experiments that produced liquids with very high Na_2O contents at low melt fractions (e.g., Robinson et al., 1998). These experiments suggest that Na_2O behaves as a highly incompatible element, partitioning strongly into the liquid phase. The pHMELTS algorithm also calculates a liquid with Na_2O contents that appear unreasonably high. Longhi (2002) proposed an alternative: that as pressure increased, the partition coefficient of Na_2O in cpx would increase, and this compatibility would serve as a barrier to the generation of high Na_2O contents in liquids from pressures above 2 GPa. Specifically, from pressures of 3 GPa higher, Longhi (2002) proposed that the liquids would be limited to about 2.5% Na_2O at the lowest melt fractions and in enriched sources. Our experiments are able to produce liquids that have measurably higher Na_2O contents than this limit; although variations in solid modal abundances cause some variation in Na_2O, our experimental values ranged from 2.6% up to 3.42% Na_2O. In context with the other elements, this behavior is unsurprising. The expansion of the olivine field and contraction of the cpx field due to the presence of water would be expected to decrease the bulk partition coefficient of Na_2O. Indeed, the cpx data in the experiments of Longhi (2002) typically show higher Na_2O contents and higher values of

D_{Na2O} than seen in our hydrous experiments. While our liquid Na_2O concentrations only mildly exceed the Longhi limit, these experiments suggest that hydrous melting and its effects on the solid relations can be expected to increase the Na_2O content of silicate liquids from depth.

Because Na_2O only makes up a small portion of the melt, it is the first element that we can analyze using the MISE procedure of Hirschmann and Dasgupta (2007) without having to worry about a large correction for closure (bringing the glass totals to 100%). When we use the measured partition coefficients for these experiments, the solid composition for KLB-1 given by Davis et al. (2009), and modal abundances calculated by mass balance, the predicted liquid should have 2.5% Na_2O, close to the range of measured compositions. However, this calculation is made more difficult by the change in cpx stability in the hydrous system; as the cpx field contracts, the modal abundance of cpx should decrease. Any attempt to take into account this decrease in cpx abundance in the MISE procedure leads to a liquid with higher Na_2O. Using the modal abundances calculated by pHMELTS which includes some opx, we calculate a liquid with over 4.0% Na_2O. This effort suggests that our Na_2O contents are not unreasonable and that a range of 2.5%-4% Na_2O likely spans much of the accessible range in Na_2O contents at these pressures, but also illustrates the difficulty of applying the MISE procedure with variable solid modal abundances and compositions.

4.5. K_2O

K_2O is the only measured oxide other than the volatiles that is perfectly incompatible at the level of the measurements applied here. K_2O varies from 0.25% to 0.5% in our liquids, but even in the most potassic experiment and with solid compositions

measured at high currents and long counting times, K_2O cannot be statistically distinguished from zero in any solid phase. Including this element in any MISE calculation produces a calculated liquid with very high K_2O contents, and therefore this calculation was not performed on this element. K_2O contents in natural liquids formed from peridotite could potentially cover a large range in compositions, with potentially corresponding effects on the other oxides in the liquid, as illustrated by the arrows in figure 9.

4.6. Cr_2O_3

Compared to the measured liquid composition in every other study from 3 GPa considered here, the Cr_2O_3 content of our liquid is lower by a significant amount. In our samples, Cr_2O_3 is incompatible in olivine, but is strongly compatible in garnet and only slightly less compatible in cpx. Despite the fact that our experiments are conducted outside the stability field of spinel, compatibility in these two phases pushes the Cr_2O_3 content of our liquid very low. We measure only 0.1-0.15% Cr_2O_3 in our liquids. The experiments of Gaetani and Grove (1998) typically also show low Cr_2O_3 contents, but many of them contain spinel, a phase in which Cr_2O_3 is compatible. None of the experiments of Walter (1998) or the calculated compositions from the BATCH algorithm of Longhi (2002) show Cr_2O_3 contents as low as our experiments. The solids measured in Walter (1998) do show Cr_2O_3 contents similar to or greater than those measured in our garnets and cpx, but overall would have slightly lower partition coefficients because of the higher liquid contents. The pHMELTS calculation also gives liquids with much higher Cr_2O_3 contents than we measured, because the algorithm does not yet include Cr_2O_3-bearing components in any solid other than spinel.

The MISE procedure suggests that our liquid compositions are consistent with the partition coefficients that we measure. Application of the MISE procedure predicts liquid compositions of 0.10 to 0.12% Cr_2O_3, very similar to the amounts measured in our experiments. Hydrous melting at high pressure therefore appears to produce liquids with very low Cr_2O_3 contents.

4.7. TiO_2

Longhi (2002) spent significant effort attempting to understand the partitioning of TiO_2 during high-pressure melting. He proposed that two major effects could explain the TiO_2 contents of low-degree melts, both related to the partitioning of TiO_2 between cpx and melt. As the cpx field expanded with increasing pressure, D_{TiO2} decreased and consequently liquid TiO_2 contents increased. Similarly, as the liquid alkali content decreased (which also correlates with increasing pressure), D_{TiO2} decreased. Because our experiments show significant changes in cpx composition and liquid sodium content associated with the presence of water, it follows that the partitioning of TiO_2 may be significantly different in our experiments from those conducted either at lower pressures or without water.

A starting point for analyzing the partitioning of TiO_2 during hydrous melting is our sub-solidus experiments, with low CaO cpx. Based on the analysis of Longhi (2002), we should expect that as CaO increases in cpx, D_{TiO2} should increase. Below the solidus temperature, we see that TiO_2 contents in the garnet and cpx are roughly similar. Garnet typically shows slightly higher TiO_2 contents than the cpx, 0.265% compared to 0.237%, but this difference is barely resolvable above the error in the analyses (~0.015%, 1σ). These values are a factor of two lower than the TiO_2 contents reported in garnet by

Walter (1998) but are similar to the TiO_2 contents reported in some of his cpx, although those measurements show considerable variability from run to run.

When the solid peridotite reacts with the liquid, the cpx field contracts as described above, and the CaO content of the cpx increases. According to the presentation of Longhi (2002), this transition should be associated with an increase in D_{TiO2} for cpx. However, our experiments consistently show the opposite behavior: D_{TiO2} decreases for cpx when the minerals are reacted with hydrous liquids. At either a constant TiO_2 content in the garnet or a constant solid TiO_2 content, D_{TiO2} is lower in the hydrous case. Our measured values of D_{TiO2} cluster between 0.15 and 0.20 (with one outlier at 0.28 in R385, the experiment with the highest liquid Na_2O and K_2O).

Longhi (2002) proposes that another key variable for determing D_{TiO2} is the alkali content of the liquid. Our liquids show higher Na_2O content than those of Longhi (2002) which, based on his work, we expect to be associated with increased D_{TiO2}. As noted, the D_{TiO2} we measure falls below the calculated value predicted by the BATCH algorithm for a cpx with the CaO content measured in our experiments. However, the measured values of D_{TiO2} fall within the range of experimental results given by Longhi (2002) at these alkali contents; it seems BATCH predicts a lower value of D_{TiO2} than shown by most of the experiments at low alkali contents. Overall, our experiments produce liquids with higher alkali contents and lower TiO_2 contents than predicted by BATCH, requiring that the bulk D_{TiO2} in our experiments is greater than predicted by the BATCH algorithm despite the decrease in D_{TiO2} for cpx. This result is due to a combination of the effect of alkalis on D_{TiO2} for cpx and the compatibility of TiO_2 in garnet, which appears to be the main host for TiO_2 during our experiments.

When the MISE procedure is used, the predicted TiO_2 content of our liquid is higher than that measured in any liquid; from 1.0 to 1.5% TiO_2 depending on the solid assemblage. This result suggests that our liquids may not have sufficient TiO_2 to equilibrate with solid KLB-1. However, if this were the case, then our solids should consistently show a decrease in TiO_2 content, a behavior that is not always true for the garnets (Table 2). The measured partition coefficients can only be reconciled with the MISE procedure if the solids have a higher proportion of garnet or if our starting material has slightly less TiO_2 than the measured KLB-1 composition given by Davis et al. (2009). It is possible that the liquid TiO_2 content is reduced slightly because the additional garnet added to the solid assemblage may have increased the bulk D_{TiO2}. For our final hydrous liquid composition we estimate a TiO_2 concentration of 0.9%, but this number is sensitive to small changes in source mineralogy.

Overall, TiO_2 partitioning appears to be a complicated function of the mineral modes, liquid composition, and solid compositions. Garnet appears to be the main host phase for TiO_2, and thus its abundance may control the initial liquid TiO_2 contents. Because of the high garnet content, our liquids have lower TiO_2 contents than the low-degree, high-pressure melt of Longhi (2002). If the correlation suggested by Longhi (2002) between liquid alkali contents and bulk D_{TiO2} is correct, it may require a correlation between D_{TiO2} for garnet and liquid alkali contents. This should be investigated in future experiments.

While attempting to model fractional crystallization and source trends for the Azores, Asimow et al. (2004) noted that the MELTS algorithm shows an increase in partition coefficient for TiO_2 in low-degree liquids, but possibly overestimates the effect.

pHMELTS calculates a higher TiO_2 content than seen in our liquids, but also includes opx in the solids, which would further decrease the D_{TiO2} and increase the TiO_2 content in the liquid. pHMELTS calculates a TiO_2 content that is not substantially different from what would be predicted using the MISE technique of Hirschmann and Dasgupta (2006). The diamond aggregate experiments of Baker et al. (1995) showed TiO_2 concentrations that are at or below the lowest values given here. The higher TiO_2 concentrations measured here are therefore consistent with the proposal of Asimow et al. (2004) that the pHMELTS model and the experiments of Baker et al. (1995) overestimate the compatibility of TiO_2 at low melt fractions.

4.8. H_2O contents and implications for mantle melting and partitioning

Our experiments are typically more hydrous than the liquids that might be expected at these temperatures from estimates of the dry solidus temperature and the magnitude of solidus depression due to water. The pHMELTS algorithm, for example, predicts liquid compositions with half as much water as we see in our average experimental liquid when the solidus is adjusted to 1375 °C. If the partition coefficient for H_2O remained near 0.01, as is expected based on some calibrations (e.g., Aubaud et al., 2004; Hirschmann et al., 2009), then the source for a liquid with 5% water would be required to have ~500 ppm H_2O. This is much higher than estimated for normal MORB source (Michael, 1988; Hirth and Kohlstedt, 1996; Gose et al., 2009) and may only be applicable to enriched, hotspot-affected, or subduction-related environments.

However, the behavior seen in our series of melting experiments is more complex than this simple partitioning model. Our experiments sample a wide variety of water contents, from 2.7% to 6.0% H_2O in the melt. Furthermore, the composition of the liquid

appears to vary with water content (Figures 8, 9, and 10). These experiments suggest that melts of varying composition can be produced in equilibrium with the solid peridotite assemblage across a variety of total water contents, and no single water content can be fully representative of the liquid in equilibrium with KLB-1 under these pressure and temperature conditions.

The contraction of the cpx field described above has very important implications for the partitioning of water during mantle melting. Based in part on measurements from the experiments of Gaetani and Grove (1998), Aubaud et al. (2004) and Hauri et al. (2006) proposed that the partitioning of water between melt and olivine or pyroxene was a strong function of the Al_2O_3 content of the solid phase due to charge-coupled substitution of H^+-Al^{3+} for Si^{4+}. Despite increased pressure, the cpx in our experiments show aluminum contents that are equal to or in many cases less than those in the experiments of Gaetani and Grove (1998). This low Al_2O_3 content appears to be caused by a combination of the contraction of the cpx field described above and the high abundance of garnet in the solids. This behavior is also consistent with the lower Al_2O_3 content of our liquid than those from lower pressures.

As our pyroxenes have lower Al_2O_3 content, the calibrations of Hauri et al. (2006) and Aubaud et al. (2004) predict that D_{H2O} in our experiments should be less than in the experiments of Gaetani and Grove (1998). While our final liquid did not equilibrate with opx, we did see opx in a previous iteration in equilibrium with a hydrous liquid, and thus we can also estimate its Al_2O_3 content based on those measurements. Both pyroxenes in our experiments showed Al_2O_3 contents between 5-6%, which in the Hauri or Aubaud calibrations would give a $D_{H2O} \sim 0.015$ for both pyroxenes (Tables 1 and 2). These values

are significantly below those used by Aubaud et al. (2004), Hauri et al. (2006), or Hirshmann et al. (2009) to estimate the storage capacity of the upper mantle and the water content of low-degree melts. Using these partition coefficients, the mineral modes calculated here, and estimates of the partition coefficient between olivine and garnet and liquid, we calculate a bulk D_{H2O} ~ 0.006, 50% lower than the value calculated by Aubaud et al. (2004) or Hirschmann et al. (2009) at pressures close to 3 GPa.

The decreasing Al_2O_3 content of pyroxenes in the garnet field seen here therefore has a number of implications for the behavior of water in the mantle. Previously the water storage capacity of the upper mantle was expected to increase with increasing depth due to the increasing Al_2O_3 content of the pyroxenes until reversing at pressures greater than 3 GPa as the modal abundance of garnet increased (Hirschmann et al., 2005; Hirschmann et al., 2009). Our experiments show lower pyroxene Al_2O_3 contents than previously measured at this pressure. If the partition coefficient D_{H2O} estimated here is accurate, it also suggests that in the upper mantle, water would be less compatible than estimated by Aubaud et al. (2004) or Hirschmann et al. (2009). Because the available pyroxenes from 2.8-3.0 GPa all contained significantly more Al_2O_3 than seen in our experiments, those authors predicted that mantle with low total water contents would only melt at depths close to the dry peridotite solidus. Our experiments show that the decreased partition coefficient for water could persist to lower pressures than previously seen, close to the spinel to garnet transition. The liquid water contents seen here could therefore still be produced by melting of a mantle with more typical water contents, possibly down to 100-200 ppm. These water contents could still provide substantial solidus depression, contrary to the suggestion of Hirschmann et al. (2009) that peridotites with ~100 ppm water would

only melt close to the dry solidus. We caution that the partition coefficient D_{H2O} could not be measured directly in our experiments because of the small grain size; the partition coefficient could only be estimated by measurement of the pyroxene Al_2O_3 content. Our experimental technique could potentially be modified using coarser-grained starting materials to allow for measurement of the actual D_{H2O} and we suggest that completing such experiments in the presence of substantial garnet is particularly important.

Several authors have attempted to estimate the bulk partition coefficient for H_2O during production of natural basalts by comparing the partitioning of water to various rare earth elements that may have similar *D* values. Michael (1995) suggested that in samples from the mid-Atlantic ridge, the partition coefficient for water was close to that of cerium. Danyushevsky et al. (2000) measured rocks from the East Pacific Rise and the Southeast Indian Ridge and made a similar comparison to Ce, but also analyzed rocks from the Lamont Seamounts west of the East Pacific Rise and found instead that the partition coefficient of water was closer to that of La, a more incompatible element. In back-arc basins, H_2O acts most like Nd, a more compatible element than Ce (Stolper and Newman, 1994). This data suggests a mechanism for this variation that was not previously known. Coupled substitution mechanisms with aluminum in pyroxenes have been proposed not just as a method for entry of water into minerals but also for a number of other elements including La and Ce (Blundy et al., 1998, and below). Since the size and charge of water (or hydrogen) is substantially different from either of those rare earth elements, it follows that the relative partitioning of these elements could change substantially over the pressure range covered by a single melting column. The change in relative partition coefficients could be due to a change in the partitioning for La, Ce, or

H_2O and may give information about the modal abundance of pyroxenes in the source, the average depth of melting, or even the temperature profile (if a substantial amount of melting occurred in the anhydrous melting regions). Thus, the decreased D_{H2O} observed in the Lamont Seamounts could be evidence for the production of those liquids at a greater average pressure than those sampled on-axis at ridges, from zones where the stability of garnet was reducing the Al_2O_3 content of any pyroxenes.

Dasgupta et al. (2007) noted that there was likely a strong interaction between carbonate-driven melting at mantle pressures up to 10 GPa and any water present in the upwelling rocks. Our hydrous melting experiments also suggest a strong interaction between water and carbonate during melting (e.g., Figure 6, Figure 8). Dasgupta et al., (2007) suggested that the presence of carbonate-rich melts deeper in an upwelling system may dehydrate the mantle source prior to reaching its hydrous solidus. If that is true, then carbonated peridotite may be expected to produce melts of a very different composition than would hydrated peridotite. Our data suggests tentatively that adding carbonate to a hydrous silicate melt may counteract some of the effect of water on the change in liquid composition by increasing the $(MgO + FeO)/SiO_2$ ratio. The strongest signature of hydrous melting, therefore, might be found in areas that have sources with either high water contents or low carbon contents, whereas high carbon contents and low water contents may be required to produce the signatures of carbonatite melting (Dasgupta and Hirschmann**,** 2007). Further experiments are required on silicate melts with a variety of ratios of carbonate to water contents to better constrain this behavior.

4.9. Additional implications of these experiments for natural melting

Our results suggest that the production of hydrated silicate liquids under mid-ocean ridges from depths several tens of kilometers greater than the dry solidus intersection along an anhydrous adiabat remains plausible. The behavior demonstrated here, including melting in the presence of garnet and the effects of the presence of water on the olivine and cpx fields can potentially have important implications for the chemistry and location of melt generation under mid-ocean ridges.

4.9.1. Presence of garnet during melting.

As discussed above in the introduction, the presence of a garnet signature in the trace element budget of mid-ocean ridge basalts presents a problem for models based on anhydrous peridotite sources. We show here that hydrous melting continues to be a possible resolution for this issue.

The proposal that hydrous melting relates to the garnet signature appears to be consistent with the major element characteristics of our liquids. Kinzler (1997) and previous workers, including Klein and Langmuir (1989), have demonstrated that the major element signatures of MORB show trends where lower melt fractions correlate with higher Na_2O contents and often higher SiO_2 contents. This chemistry is qualitatively consistent with the patterns observed here in hydrous melting; the addition of water during melting both decreases the partition coefficient D_{Na2O} and also produces a liquid with elevated SiO_2. The melts that have the highest Na_2O contents are also those which typically show the strongest garnet signature as well (Shen and Forsyth, 1995). Longhi (2002) shows that at pressures above the spinel-to-garnet transition, Na_2O should become significantly more compatible in cpx during anhydrous melting. In the case of anhydrous melting, therefore, it could be particularly difficult to reconcile the high liquid Na_2O

contents with the presence of garnet, as the liquids produced in the garnet field would be expected to have lower Na_2O contents.

The presence of water during melting offers a possible explanation for the garnet signature and the associated correlations in a number of ways. First, hydrous melts are typically expected to be only low-degree melts which sample a large portion of the available water but do not produce large melt volumes. In this way, a hydrous melt can potentially explain the correlation between the increasing garnet signature and decreasing degree of melting (Shen and Forsyth, 1995). Asimow and Langmuir (2003) calculated that for a constant total amount of melt production represented by a constant crustal thickness, increasing the water content of the source led to a decrease in the average degree of melting represented by the final accumulated liquid, because the additional water led to a larger amount of low-degree hydrous melts being sampled. If these low degree melts were generated in the garnet field, they would carry the garnet signature, and therefore the wettest and coldest sources would produce melts of the lowest average melt fraction and could also carry the strongest garnet signatures.

Based on anhydrous experiments, Robinson and Wood (1998) argued that the spinel-to-garnet transition occurs in the range of 2.5-3.0 GPa in most peridotites, and that production of significant quantities of melt from the garnet field would require melting to begin at even greater pressures, up to 3.5 GPa, with potential temperatures that would generate an implausibly large amount of melt. However, they also conducted sub-solidus experiments and showed that the temperature of the spinel to garnet transition was strongly pressure dependent, with a slope of ~400 °C per GPa. For the temperature used in our experiments, ~1375 °C, extrapolation of their given phase boundary predicts a

spinel to garnet transition of ~2.5 GPa. As melting proceeds, the temperature of the assemblage would decrease as energy is converted to latent heat, and thus the beginning of melting could push the spinel-to-garnet transition to even lower pressures. The experiments of Gaetani and Grove (1998) produced measureable garnet at pressures as low as 1.6 GPa and temperatures as low as 1255 °C. As noted by Gaetani and Grove (1998), water fluxes peridotite melting at lower temperatures than would otherwise occur, and therefore water-driven melting is much more likely to occur within the garnet field and could maintain garnet in the source to much shallower pressures than could be sampled by anhydrous melts.

The partitioning of the rare earth elements and radioactive isotopes has been a key part of the debate over the presence or absence of the garnet signature. Garnet is believed to be the main phase able to retain the heavy rare earth elements (HREE) during melting, and therefore a depleted HREE signature is typically interpreted as a major sign of garnet in the source (e.g., Stolper and Hirschmann, 1996). Compatibility of radioactive elements such as Lu or U can also yield garnet signatures in isotope ratios by fractionating parent and daughter isotopes (e.g., Salters and Hart, 1989). The attribution of such signatures to garnet requires that garnet is the only common phase in the melting zone able to fractionate these elements in the correct sense during melting. Wood et al. (1999) and Blundy et al. (1998) argued that this was not the case by measuring partition coefficients for the key elements, including the HREE and U in aluminous cpx that were significantly greater than those measured elsewhere. The increased compatibility of those elements in cpx at pressure could therefore explain the presence of a so-called garnet signature in liquids produced without the presence of garnet.

Our cpx compositions have important implications for this issue. In the experiments of Wood et al. (1999) and Blundy et al. (1998) where increased partitioning of these elements into cpx was observed, the cpx compositions were highly aluminous, and the substitution mechanism proposed for these elements was a coupled-substitution involving Na^{+} and Al^{3+}. Our hydrous experiments show cpx with much lower Na and Al contents due to the presence of garnet and the contraction of the cpx field in the presence of a hydrous melt. The experiments of Gaetani and Grove (1998) were conducted at similar pressures to the experiment of Blundy et al. (1998) and also produced cpx with lower Al_2O_3 contents than Blundy et al. (1998), suggesting that the highly aluminous cpx required to explain the production of a garnet signature may only occur in anhydrous systems. These hydrous experiments suggest that if significant water is present during melting, the garnet signature cannot be produced by the presence of cpx under these conditions because of the reduced aluminum content of the cpx.

An illustrative example can be found in TiO_2 concentrations. As discussed previously, the contraction of the cpx field seen here led to decreasing TiO_2 contents in the cpx compared to the sub-solidus cpx with higher Al_2O_3 content. Blundy et al. (1998) reported a cpx with 10.47% Al_2O_3 and 0.74% TiO_2 in equilibrium with a melt from lower pressures containing 1.15% TiO_2. While their liquid TiO_2 content is only slightly higher than our predicted liquid, the TiO_2 content of their cpx is a factor of 3-5 greater than we measure and consequently our experiments show a D_{TiO2} for cpx that is also a factor of 3-5 lower than the experiment of Blundy et al. (1998). Although we did not measure trace elements in our experiments, a similar effect on the remaining incompatible elements such as the HREE would mean that during hydrous melting, garnet would be the only

phase capable of creating the trace element and isotopic signatures typically referred to as the garnet signature.

Hirschmann and Stolper (1996) and Pertermann and Hirschmann (2003b) hypothesized that an alternate explanation for the presence of the garnet signature could be the presence of small amounts of pyroxenite in the melting source. Pertermann and Hirschmann (2003b) estimated the magnitude of the typical garnet signature could be explained by ~2% pyroxenite in the MORB source. This suggestion remains a plausible alternate mechanism for generation of the garnet signature that cannot be ruled out by this work, although the observed effect of water-rich melts on the stability field of cpx could have important implications for melting of pyroxenites. We will consider some of the major element implications here and a specific example of minor element signatures in Chapter 3.

4.9.2. Pyroxenitic sources

If the contraction of the cpx field during hydrous melting were a general phenomenon, it potentially has important implications for the melting of variable source lithologies.

Melts of variable calcium contents have been observed from many systems, from very low values up to the very high concentrations in those melts termed ultra-calcic (Kogiso and Hirschmann, 2001). An increasingly fertile source would be expected to have higher cpx abundances than a depleted source, and would also be expected to be more hydrous. Thus, the cpx in an enriched source may be expected to show a stronger contraction of the cpx field alongside a greater modal abundance of cpx. Melting of a hydrous, enriched source may be a method of producing particularly low CaO contents in

liquids that maintain a garnet signature in the trace elements, as the calcium may be more compatible if the source material contains a large quantity of high-CaO cpx. Conversely, it appears extremely difficult to produce liquids with a high CaO content if water is present, forcing the cpx to high CaO contents. Other processes, such as high temperature, carbon-fluxed melting, or high-degree melting of non-peridotite sources may be necessary to produce ultra-calcic liquids. Wet melting could produce moderately elevated CaO contents by reducing the modal abundance of cpx, as seen in our experiments, but the presence of highly calcic cpx could impose an upper limit on the liquid CaO content.

As shown above, the TiO_2 content of liquids can be a particularly strong function of the abundance and composition of the cpx in the solid. The extreme of this behavior is found in the case of melting of a pyroxenite. Pertermann and Hirschmann (2003a) produced very high TiO_2 (up to 6.7%) coexisting with a high-Al_2O_3 cpx If these melts were hydrous and the D_{TiO2} for cpx decreased further, the resulting liquid could be even richer in TiO_2. High liquid TiO_2 concentrations may therefore be a method of identifying contributions from hydrous melting of pyroxenite sources.

4.9.3. Liquid alkali contents

Previously, melting experiments on both peridotite and pyroxenite-rich lithologies produced liquids that tend to decrease in Na_2O content with increasing pressure (Longhi, 2002; Yaxley et al., 2007). Ideally, this would create a situation where the ratio of K_2O/Na_2O in MORB could be interpreted as an indicator of the initial pressure of melting. However, this method has not been particularly effective at predicting pressures (Yaxley et al., 2007). Our experiments suggest that a major complication to any simple explanation of the alkali ratios of a liquid may be the presence of water in its source. If

hydrous melting contracts the stability field of cpx, then it is expected to have the opposite effect of increasing pressure on the partition coefficient for Na_2O; increasing pressure would increase D_{Na2O} while increasing water content would decrease D_{Na2O}. Since hydrous melts are expected to be produced at higher pressures than anhydrous melts, these two effects would interact and potentially create very complicated relationships between the liquid and solid Na_2O contents, pressure, and composition. Hydrous melting of pyroxenite lithologies in particular could be expected to show elevated Na_2O if the effects of water on cpx are similar to those seen in peridotite, in the opposite direction of the simple relationship between K_2O/Na_2O and pressure.

As noted above, K_2O is essentially perfectly incompatible in our experiments. Based on these experiments, K_2O can then be treated either as a tracer of source enrichment or of the volume of source sampled. Asimow and Langmuir (2003) showed that hydrous melting under a mid-ocean ridge could increase the volume of mantle sampled by producing a low-degree melt at greater depths and in rocks that typically would remain sub-solidus had water not been present. Therefore, the presence of water might be expected to increase the potassium content of erupted liquids at mid-ocean ridges by increasing the volume of peridotite that melts. Alternatively, K_2O and water contents in enriched sources would be expected to increase together (Asimow et al., 2004). Increased potassium in liquids may be expected to show interesting correlations with other indicators of source enrichment, and isolating either of these effects in natural MORB may require detailed modeling.

5. CONCLUSION

The presence of water during melting at 3GPa produces liquids with an increased SiO_2 content and a decreased (MgO+FeO)/SiO_2 ratio compared to anhydrous melts from the same pressure, consistent with the results from hydrous melting experiments at lower pressures. This effect is tantamount to increasing the stability field of olivine relative to the other phases present. The presence of a hydrous melt also has a strong effect on the composition of the equilibrium clinopyroxene. Anhydrous clinopyroxenes from this pressure show high Al_2O_3 contents, while our hydrous clinopyroxenes show elevated CaO contents and lower Al_2O_3 contents than seen in any anhydrous experiment from this pressure. The clinopyroxene composition field therefore contracts substantially due to the presence of water. Trace elements which may be hosted in the mantle by clinopyroxene through coupled substitutions involving Al_2O_3, including water, will therefore have lower partition coefficients during hydrous melting than during anhydrous melting, and these reduced partition coefficients will strongly affect the water content and the trace element characteristics of any melt produced at this pressure.

6. ACKNOWLEDGEMENTS

This work benefited from many enlightening discussions with Sally Newman, George Rossman, Mark Hirschmann, Liz Muira, Ma Chi, and Mike Baker. The authors would like to thank Alex Sessions and Magnus Eek for the use of their Elemental Analyzer and Ed Stolper and John Beckett for the use of their 1-atmosphere furnaces. This work was supported by the NSF Ocean Sciences Marine Geology and Geophysics program, grant numbers OCE-0241716 and OCE-0550216.

References

Asimow, P. D., Hirschmann, M. M., Ghiorso, M. S., and Stolper, E. M. (1999) Calculation of peridotite partial melting from thermodynamic models of minerals and melts. III. Controls on isobaric melt production and the effect of water on melt production. *J. Petrol.* **40**, 831-851.

Asimow, P. D. and Langmuir, C. H. (2003) The importance of water to oceanic mantle melting regimes. *Nature* **421**, 815-820.

Asimow, P. D., Dixon, J. E., and Langmuir, C. H. (2004) A hydrous melting and fractionation model for mid-ocean ridge basalts: application to the Mid-Atlantic Ridge near the Azores. *Geochem. Geophys. Geosyst.* **5**, Q01E16.

Aubaud, C., Hauri, E. H., and Hirschmann, M. M. (2004) Hydrogen partition coefficients between nominally anhydrous minerals and basaltic melts. *Geophys. Res. Lett.* **31**, L20611.

Aubaud, C., Withers, A. C., Hirschmann, M. M., Guan, Y., Leshin, L. A., Mackwell, S. J., and Bell, D. R. (2007) Intercalibration of FTIR and SIMS for hydrogen measurement in glasses and nominally anhydrous minerals. *Am. Mineral.* **92**, 811-828.

Baker, M. B. and Stolper, E. M. (1994) Determining the composition of high-pressure mantle melts using diamond aggregates. *Geochim. Cosmochim. Ac.* **58**, 2811-2827.

Baker, M. B., Hirschmann, M. M., Ghiorso, M. S., and Stolper, E. M. (1995) Compositions of near-solidus peridotite melts from experiments and thermodynamic calculations. *Nature* **375**, 308-311.

Bishop, J., Madejová, J., Komadel, P., and Fröschl, H. (2002) The influence of structural Fe, Al and Mg on the infrared OH bands in spectra of dioctahedral smectites. *Clay Minerals* **37**, 607-616.

Blundy, J. D., Robinson, J. A. C., and Wood, B. J. (1998) Heavy REE are compatible in clinopyroxene on the spinel lherzolite solidus. *Earth Planet Sc. Lett.* **160**, 493-504.

Chou, I. (1986) Permeability of precious metals to hydrogen at 2 kb total pressure and elevated temperatures. *Am. J. Sci.* **286**, 638-658.

Danyushevsky, L. V., Eggins, S. M., Falloon, T. J., and Christie, D. M. (2000) H_2O abundance in depleted to moderately enriched mid-ocean ridge magmas; part I: incompatible behaviour, implications for mantle storage, and origin of regional variations. *J. Petrology* **41**, 1329-1364.

Dasgupta, R. and Hirschmann, M. (2007) A modified iterative sandwich method for determination of near-solidus partial melt compositions. II. Application to determination of near-solidus melt compositions of carbonated peridotite. *Contrib. Mineral. Petr.* **154**, 647-661.

Dasgupta, R., Hirschmann, M. M., and Smith, N. D. (2007) Water follows carbon: CO_2 incites deep silicate melting and dehydration beneath mid-ocean ridges. *Geology* **35**, 135-138.

Davis, F. A., Tangeman, J. A., Tenner, T. J., and Hirschmann, M. M. (2009) The composition of KLB-1 peridotite. *Am. Mineral.* **94**, 176-180.

Dixon, J. E., Stolper, E. M., and Holloway, J. R. (1995) An experimental study of water and carbon dioxide solubilities in mid ocean ridge basaltic liquids.1. Calibration and solubility models. *J. Petrol.* **36**, 1607-1631.

Falloon, T. J. and Danyushevsky, L. V. (2000) Melting of refractory mantle at 1.5, 2, and 2.5 GPa under anhydrous and H_2O-undersaturated conditions: implications for the petrogenesis of high-Ca boninites and the influence of subduction components on mantle melting. *J. Petrol.* **41**, 257-283.

Fine, G. and Stolper, E. M. (1986) Dissolved carbon dioxide in basaltic glasses: concentrations and speciation. *Earth Planet Sc. Lett.* **76**, 263-278.

Gaetani, G. A. and Grove, T. L. (1998) The influence of water on melting of mantle peridotite. *Contrib. Mineral. Petr.* **131**, 323-346.

Gose, J., Schmadicke, E., and Beran, A. (2009) Water in enstatite from Mid-Atlantic Ridge peridotite: evidence for the water content of suboceanic mantle? *Geology* **37**, 543-546.

Hauri, E. H., Gaetani, G. A., and Green, T. H. (2006) Partitioning of water during melting of the Earth's upper mantle at H_2O-undersaturated conditions. *Earth Planet Sc. Lett.* **248**, 715-734.

Herzberg, C. (2000) New experimental observations on the anhydrous solidus for peridotite KLB-1. *Geochem. Geophys. Geosyst.* **1**, 1051.

Herzberg, C. (2006) Petrology and thermal structure of the Hawaiian plume from Mauna Kea volcano. *Nature* **444**, 605-609.

Hirose, K. and Kushiro, I. (1993) Partial melting of dry peridotites at high pressures - determination of compositions of melts segregated from peridotite assemblage using aggregates of diamond. *Earth Planet Sc. Lett.* **114**, 477-489.

Hirschmann, M. M. and Stolper, E. M. (1996) A possible role for garnet pyroxenite in the origin of the "garnet signature" in MORB. *Contrib. Mineral. Petr.* **124**, 185-208.

Hirschmann, M. M., Aubaud, C., and Withers, A. C. (2005) Storage capacity of H_2O in nominally anhydrous minerals in the upper mantle. *Earth Planet Sc. Lett.* **236**, 167-181.

Hirschmann, M. M. and Dasgupta, R. (2007) A modified iterative sandwich method for determination of near-solidus partial melt compositions. I. Theoretical considerations. *Contrib. Mineral. Petr.* **154**, 635-645.

Hirschmann, M. M., Tenner, T., Aubaud, C., and Withers, A. C. (2009) Dehydration melting of nominally anhydrous mantle: the primacy of partitioning. *Phys. Earth Planet In.* **176**, 54-68.

Hirth, G. and Kohlstedt, D. L. (1996) Water in the oceanic upper mantle: implications for rheology, melt extraction and the evolution of the lithosphere. *Earth Planet Sc. Lett.* **144**, 93-108.

Holloway, J. and Kawamoto, T. (1997) Melting temperature and partial melt chemistry of H_2O-saturated mantle peridotite to 11 gigapascals. *Science* **276**, 240-243.

Humayun, M., Qin, L., and Norman, M. D. (2004) Geochemical evidence for excess iron in the mantle beneath Hawaii. *Science* **306**, 91-94.

Iwamori, H., McKenzie, D., and Takahashi, E. (1995) Melt generation by isentropic mantle upwelling. *Earth Planet Sc. Lett.* **134**, 253-266.

Johnson, K. T. M. and Kushiro, I. (1992) Segregation of high-pressure partial melts from peridotite using aggregates of diamond - a new experimental approach. *Geophys. Res. Lett.* **19**, 1703-1706.

Kägi, R., Muntener, O., Ulmer, P., and Ottolini, L. (2005) Piston-cylinder experiments on H_2O undersaturated Fe-bearing systems: an experimental setup approaching $f(O_2)$ conditions of natural calc-alkaline magmas. *Am. Mineral.* **90**, 708-717.

Kelemen, P. B., Dick, H. J. B., and Quick, J. E. (1992) Formation of harzburgite by pervasive melt/rock reaction in the upper mantle. *Nature* **358**, 635-641.

Kessel, R., Beckett, J. R., and Stolper, E. M. (2001) Thermodynamic properties of the Pt-Fe system. *Am. Mineral.* **86**, 1003-1014.

Kinzler, R. J. (1997) Melting of mantle peridotite at pressures approaching the spinel to garnet transition: application to mid-ocean ridge basalt petrogenesis. *J. Geophys. Res.* **102**, 853-874.

Klein, E. M. and Langmuir, C. H. (1989) Local versus global variations in ocean ridge basalt composition: A Reply. *J. Geophys. Res.* **94**, 4241–4252.

Kogiso, T. and Hirschmann, M. M. (2001) Experimental study of clinopyroxenite partial melting and the origin of ultra-calcic melt inclusions. *Contrib. Mineral. Petr.* **142**, 347-360.

Kushiro, I. (1968) Compositions of magmas formed by partial melting of the Earth's upper mantle. *J. Geophys. Res.* **73**, 619-634.

Kushiro, I. (1969) System forsterite-diopside-silica with and without water at high pressures. *Am. J. Sci.* **267A**, 269-294.

Kushiro, I. (1972) Effect of water on the composition of magmas formed at high pressures. *J. Petrol.* **13**, 311-334.

Kushiro, I. and Hirose, K. (1992) Experimental-determination of composition of melt formed by equilibrium partial melting of peridotite at high-pressures using aggregates of diamond grains. *Proceedings of the Japan Academy Series B-Physical and Biological Sciences* **68**, 63-68.

Liu, X., O'Neill, H. S. C., and Berry, A. J. (2006) The effects of small amounts of H_2O, CO_2 and Na_2O on the partial melting of spinel lherzolite in the system CaO-MgO-Al_2O_3-SiO_2 +/- H_2O +/- CO_2 +/- Na_2O at 1.1 GPa. *J. Petrol.* **47**, 409-434.

Longhi, J. and Bertka, C. M. (1996) Graphical analysis of pigeonite-augite liquidus equilibria. *Am. Mineral.* **81**, 685-695.

Longhi, J. (2002) Some phase equilibrium systematics of lherzolite melting: I. *Geochem. Geophys. Geosyst.* **3**, 1020.

Michael, P. J. (1988) The concentration, behavior and storage of H_2O in the suboceanic upper mantle: implications for mantle metasomatism. *Geochim. Cosmochim. Ac.* **52**, 555-566.

Michael, P. J. (1995) Regionally distinctive sources of depleted MORB - evidence from trace-elements and H_2O. *Earth Planet Sc. Lett.* **131**, 301-320.

Mosenfelder, J. L., Deligne, N. I., Asimow, P. D., and Rossman, G. R. (2006) Hydrogen incorporation in olivine from 2-12 GPa. *Am. Mineral.* **91**, 285-294.

Mysen, B. O., Virgo, D., Harrison, W. J., and Scarfe, C. M. (1980) Solubility mechanism of H_2O in silicate melts at high pressures and temperatures: a Raman spectroscopic study. *Am. Mineral.* **65**, 900-914.

Ohlhorst, S., Behrens, H., and Holtz, F. (2001). Compositional dependence of molar absorptivities of near-infrared OH^- and H_2O bands in rhyolitic to basaltic glasses. *Chem. Geol.* **174**, 5-20.

Parman, S. W. and Grove, T. L. (2004) Harzburgite melting with and without H_2O: experimental data and predictive modeling. *J. Geophys. Res.* **109**, B02201.

Pertermann, M. and Hirschmann, M. M. (2003a) Anhydrous partial melting experiments on MORB-like eclogite: phase relations, phase compositions and mineral-melt partitioning of major elements at 2-3 GPa. *J. Petrol.* **44**, 2173-2201.

Pertermann, M. and Hirschmann, M. M. (2003b) Partial melting experiments on a MORB-like pyroxenite between 2 and 3 GPa: constraints on the presence of pyroxenite in basalt source regions from solidus location and melting rate. *J. Geophys. Res.* **108**, 2125.

Putirka, K., Johnson, M., Kinzler, R., Longhi, J., and Walker, D. (1996) Thermobarometry of mafic igneous rocks based on clinopyroxene-liquid equilibria, 0–30 kbar. *Contrib. Mineral. Petr.* **123**, 92-108.

Robinson, J. A. C. and Wood, B. J. (1998) The depth of the spinel to garnet transition at the peridotite solidus. *Earth Planet Sc. Lett.* **164**, 277-284.

Robinson, J. A. C., Wood, B. J., and Blundy, J. D. (1998) The beginning of melting of fertile and depleted peridotite at 1.5 GPa. *Earth Planet Sc. Lett.* **155**, 97-111.

Salters, V. J. M. and Hart, S. R. (1989) The hafnium paradox and the role of garnet in the source of mid-ocean-ridge basalts. *Nature* **342**, 420-422.

Salters, V. J. M. and Longhi, J. (1999) Trace element partitioning during the initial stages of melting beneath mid-ocean ridges. *Earth Planet Sc. Lett.* **166**, 15-30.

Schwab, B. E. and Johnston, A. D. (2001) Melting systematics of modally variable, compositionally intermediate peridotites and the effects of mineral fertility. *J. Petrology* **42**, 1789-1811.

Shen, Y. and Forsyth, D. W. (1995) Geochemical constraints on initial and final depths of melting beneath mid-ocean ridges. *J. Geophys. Res.* **100**, 2211–2237.

Smith, P. M. and Asimow, P. D. (2005) Adiabat_1ph: A new front end to the MELTS, pMELTS, and pHMELTS models. *Geochem. Geophys. Geosyst.* **6**, Q02004.

Stolper, E. (1980) A phase diagram for mid-ocean ridge basalts: preliminary results and implications for petrogenesis. *Contrib. Mineral. Petr.* **74**, 13-27.

Stolper, E. and Newman, S. (1994) The role of water in the petrogenesis of Mariana Trough magmas. *Earth Planet Sc. Lett.* **121**, 293-325.

Takahashi, E. and Kushiro, I. (1983) Melting of a dry peridotite at high pressures and basalt magma genesis. *Am. Mineral.* **69**, 859-879.

Toplis, M. J. (2005) The thermodynamics of iron and magnesium partitioning between olivine and liquid: criteria for assessing and predicting equilibrium in natural and experimental systems. *Contrib. Mineral. Petr.* **149**, 22-39.

Tsuchiyama, A., Nagahara, H., and Kushiro, I. (1981) Volatilization of sodium from silicate melt spheres and its application to the formation of chondrules. *Geochim. Cosmochim. Ac.* **45**, 1357-1367.

Wallace, M. E. and Green, D. H. (1988) An experimental determination of primary carbonatite magma composition. *Nature* **335**, 343-346.

Walter, M. J. (1998) Melting of garnet peridotite and the origin of komatiite and depleted lithosphere. *J. Petrology* **39**, 29-60.

Wasylenki, L., Baker, M., Kent, A., and Stolper, E. (2003) Near-solidus melting of the shallow upper mantle: partial melting experiments on depleted peridotite. *J. Petrol.* **44**, 1163-1191.

White, R. S., McKenzie, D., and O'Nions, R. K. (1992) Oceanic crustal thickness from seismic measurements and rare earth element inversions. *J. Geophys. Res.* **97**, 19683-19715.

Wood, B. J., Blundy, J. D., and Robinson, J. A. C. (1999) The role of clinopyroxene in generating U-series disequilibrium during mantle melting. *Geochim. Cosmochim. Ac.* **63**, 1613-1620.

Yaxley, G. and Sobolev, A. (2007) High-pressure partial melting of gabbro and its role in the Hawaiian magma source. *Contrib. Mineral. Petr.* **154**, 371-383.

TABLES

Table 1:	Na_2O	MgO	Al_2O_3	SiO_2	K_2O	CaO	TiO_2	NiO	MnO
CPX	1.98(9.1)	19.79(88)	6.85(35)	53.54(73)	0.00(0.5)	12.82(53)	0.26(1.6)	0.07(2.4)	0.10(1.4)
Olivine	0.03(1.1)	49.07(83)	0.13(14)	40.91(76)	0.00(0.4)	0.18(6.8)	0.007(0.6)	0.32(8.6)	0.10(1.7)
Garnet	0.03(2.2)	22.46(25)	22.29(28)	42.64(44)	0.00(0.7)	4.75(13)	0.23(1.5)	0.02(1.6)	0.19(1.7)
Az Gt	0.03(1.1)	20.67(66)	23.30(35)	41.83(68)	0.0(0.6)	4.22(9.2)	0.076(1.8)	0(2.3)	0.32(2.5)
R377 OPX	0.33(3.4)	31.30(21)	5.642(27)	55.60(28)	0.00(0.3)	1.90(9.1)	0.063(0.6)	0.01(1.7)	0.10(1.9)

Continued:	FeO	Cr_2O_3	Totals	Mg#	Modal Abundance
CPX	4.19(19)	0.54(3.2)	100.20(71)	0.893	0.30(2)
Olivine	9.87(61)	0.05(1.9)	100.74(64)	0.898	0.62(4)
Garnet	6.66(11)	0.87(4.6)	100.21(66)	0.857	0.08(4)
Az Gt	8.86(37)	0.30(2.5)	99.66(128)	0.805	
R377 OPX	6.06(23)	0.45(5.4)	101.51(26)	0.901	

Table 1: Measured compositions of solid phases from sub-solidus recrystallized peridotites. Modal Abundance calculated by least squares fit to the bulk composition of KLB-1 given by Davis et al. (2009). The AZ garnet shows the composition of the garnet seed

that was added in small amounts to the peridotite mixture before recrystallization to overcome any nucleation issues. Modal abundances were calculated via least squares fit to the measured compositions. The opx from R377 comes from an earlier step in the iteration and is given to show the composition of opx seen with these hydrous melts. Values in parentheses are 100 * the standard deviation of the electron microprobe analyses, except in the modal abundance column, which is calculated. The variation in modal abundance was calculated by Monte Carlo simulation carrying through the variance in the electron probe measurements and in the bulk composition as given by Davis et al. (2009).

Table 2: experimental results

R385	Na_2O	P_2O_5	MgO	Al_2O_3	SiO_2	K_2O	CaO	TiO_2	NiO	MnO
Liq	3.23(10)	0.00(0.7)	13.40(7.9)	12.71(10)	45.38(29)	0.49(2.7)	9.05(6.2)	0.80(2.4)	0.00(1.8)	0.15(0.6)
Ol	0.02(0.3)	0.00(0.6)	47.71(59)	0.05(1.8)	40.86(12)	0.00(0.3)	0.23(2.4)	0.00(0.5)	0.02(0.8)	0.13(0.5)
Gt	0.04(1.1)	0.00(0.8)	18.76(70)	22.91(22)	42.09(18)	0.00(0.2)	6.13(38)	0.28(6.6)	0.00(0.6)	0.24(0.9)
CPX	1.87(14)	0.01(0.7)	17.24(70)	5.79(43)	53.09(53)	0.00(0.6)	17.44(76)	0.23(9.5)	0.00(0.7)	0.10(0.7)
R390										
Liq	2.78(14)	0.01(1.2)	13.43(6.8)	12.52(12)	43.77(19)	0.44(1.6)	9.85(6.7)	0.72(2.1)	0.02(2.1)	0.16(0.5)
Ol	0.01(0.4)	0.00(0.1)	47.07(19)	0.04(1.8)	40.81(13)	0.00(0)	0.17(1.9)	0.00(0)	0.03(1.2)	0.13(0.7)
Gt	0.02(0.3)	0.01(0.9)	17.21(48)	22.44(19)	41.84(29)	0.00(0.3)	6.99(34)	0.21(3.1)	0.00(0.4)	0.23(0.9)
CPX	1.43(2.4)	0.01(0.6)	17.56(13)	5.35(17)	53.36(37)	0.00(0.3)	17.95(54)	0.12(1.1)	0.00(0.3)	0.10(0.7)
R395										
Liq	2.69(12)	0.01(1.1)	14.47(13)	12.57(13)	45.47(33)	0.37(1.9)	9.49(9.1)	0.69(1.1)	0.00(0.9)	0.14(0.5)
Ol	0.01(3.9)	0.00(0.5)	48.84(12)	0.26(10)	41.36(13)	0.00(0.2)	0.31(30)	0.00(0.4)	0.04(0.9)	0.12(0.3)
Gt	0.02(0.3)	0.00(0.9)	19.57(17)	22.92(31)	42.55(28)	0.00(0)	6.28(14)	0.23(0.0)	0.00(1.2)	0.22(0.5)
CPX	1.39(0.7)	0.01(0.7)	19.03(39)	5.08(19)	53.58(21)	0.00(0.1)	16.05(26)	0.10(8.3)	0.00(0.6)	0.10(0.9)
R389										
Liq	2.46(10)	0.00(1.1)	14.09(24)	13.0(10)	45.29(26)	0.38(3.1)	9.70(6.3)	0.68(1.8)	0.01(1.8)	0.15(0.7)
Ol	0.00(3.7)	0.00(0.6)	47.80(96)	0.03(35)	40.73(42)	0.00(0.2)	0.17(46)	0.00(3.1)	0.01(0.9)	0.13(0.8)
Gt	0.03(6.7)	0.00(0.1)	19.28(43)	22.24(46)	42.12(15)	0.00(0.5)	6.47(81)	0.16(0.9)	0.00(0.2)	0.24(0.3)
CPX	1.10(0.2)	0.00(0.1)	18.04(18)	5.19(1.0)	53.08(7.2)	0.00(0.2)	17.03(0.8)	0.13(0)	0.00(0.7)	0.11(0.2)
R398										
Liq	2.76(1.1)	0.01(0.9)	14.81(34)	12.47(11)	44.69(53)	0.43(0.3)	9.52(23)	0.67(6.2)	0.00(1.8)	0.15(1.8)
Ol	0.00(4.8)	0.00(0.7)	50.14(21)	0.03(6.3)	40.42(25)	0.00(0.3)	0.20(51)	0.00(1.1)	0.01(1.4)	0.12(0.7)
Gt	0.02(0.6)	0.01(0.7)	20.51(54)	22.75(1.8)	41.63(58)	0.00(0)	6.55(3.3)	0.20(0.0)	0.01(1.4)	0.22(0.9)
CPX	1.25(20)	0.02(1.3)	18.74(29)	5.07(14)	53.01(40)	0.00(4.4)	17.27(9.0)	0.10(1.8)	0.01(1.5)	0.09(0.7)
R396										

Liq	2.86(1.1)	0.01(0.5)	13.95(33)	13.01(13)	43.69(27)	0.34(0.2)	9.52(20)	0.74(2.5)	0.00(1.7)	0.14(0.8)
Ol	0.01(0.6)	0.00(1.1)	48.22(53)	0.07(6.4)	40.41(23)	0.00(0.1)	0.27(16)	0.00(0.5)	0.05(1.4)	0.12(1.0)
Gt	0.01(2.3)	0.00(1.1)	20.43(26)	23.01(16)	41.91(21)	0.00(0.3)	6.26(34)	0.17(1.1)	0.00(0.8)	0.23(1.9)
CPX	1.21(6.6)	0.01(2.0)	18.16(15)	5.81(8.7)	52.96(40)	0.00(1.4)	16.93(7.5)	0.12(1.8)	0.00(1.3)	0.09(0.8)
R380IC										
IC Liq	2.47(0.8)	0.01(0.7)	15.15(56)	11.61(24)	44.11(26)	0.23(0.2)	8.11(3.2)	0.54(0.3)	0.01(2.0)	0.12(1.3)
IC OL	0.01(1.1)	0.00(0.9)	46.35(78)	0.11(40)	40.51(35)	0.00(0.3)	0.18(59)	0.00(5.4)	0.05(1.6)	0.10(1.7)
IC GT	0.02(9.9)	0.00(1.5)	19.18(16)	22.60(12)	41.60(27)	0.00(1.9)	5.68(12)	0.22(2.2)	0.01(1.6)	0.20(1.4)
R380OC										
Liq	2.83(1.0)	0.00(1.0)	14.56(22)	12.41(2.4)	44.64(19)	0.32(0.3)	9.30(1.7)	0.64(0.3)	0.00(1.3)	0.14(0.8)
Ol	0.01(3.8)	0.00(0.9)	48.18(54)	0.06(62)	40.73(45)	0.00(0.2)	0.20(41)	0.00(9.3)	0.03(1.2)	0.11(1.4)
Gt	0.04(3.9)	0.01(1.2)	20.30(19)	21.96(23)	42.11(43)	0.00(0.4)	6.17(25)	0.20(2.1)	0.00(0.8)	0.21(1.6)
CPX	1.17(11)	0.01(3.2)	18.79(39)	5.52(9.9)	52.91(10)	0.00(1.4)	15.96(12)	0.10(2.7)	0.00(0.5)	0.10(2.2)
R393 IC										
Liq	2.47(0.8)	0.01(1.0)	13.26(54)	11.91(8.6)	43.67(30)	0.26(0.4)	8.83(3.9)	0.59(0.6)	0.02(2.3)	0.15(1.5)
Ol	0.01(1.2)	0.00(1.1)	46.62(53)	0.08(25)	40.52(24)	0.00(0.3)	0.20(40)	0.00(3.3)	0.04(0.9)	0.11(1.7)
Gt	0.01(10.0)	0.01(1.6)	20.06(61)	22.60(20)	42.15(22)	0.00(2.2)	5.27(34)	0.14(4.2)	0.00(2.7)	0.20(2.2)
R393OC										
Liq	2.87(7.7)	0.01(1.8)	14.06(8.6)	12.75(11)	44.37(18)	0.38(1.3)	9.34(6.5)	0.72(1.1)	0.02(1.6)	0.15(0.6)
Ol	0.01(0.6)	0.01(0.2)	48.63(23)	0.05(0.8)	40.76(10)	0.00(0.2)	0.21(4.2)	0.00(0.2)	0.03(1.0)	0.12(0.1)
Gt	0.01(0.8)	0.01(0.7)	19.89(43)	22.91(7.4)	42.11(13)	0.00(0.2)	6.13(21)	0.21(5.0)	0.00(0.6)	0.22(0.8)
CPX	1.26(3.9)	0.01(0.9)	18.58(19)	5.57(8.1)	52.96(7.0)	0.00(0.3)	16.64(14)	0.13(1.0)	0.01(1.0)	0.10(0.6)

Table 2 continued:

R385	FeO	Cr_2O_3	Oxide Totals	Mg#	K_D	H_2O	CO_3	Liquid totals
Liq	9.12(12)	0.08(2.7)	95.38(45)	0.72		5.53	0.24	101.16

Ol	11.35(28)	0.02(1.9)	100.44(26)	0.88	0.35			
Gt	9.25(59)	0.33(18)	100.08(27)	0.78				
CPX	4.34(29)	0.22(21)	100.40(43)	0.87				
R390								
Liq	10.36(11)	0.10(1.9)	94.28(22)	0.70		5.37	0.28	99.94
Ol	12.30(36)	0.03(0.7)	100.64(8)	0.87	0.34			
Gt	10.71(68)	0.87(12)	100.58(23)	0.74				
CPX	4.39(33)	0.36(7.8)	100.68(16)	0.88				
R395								
Liq	7.24(12)	0.12(1.1)	93.31(57)	0.78		5.31	0.32	98.95
Ol	9.66(42)	0.04(7.3)	100.67(49)	0.90	0.38			
Gt	8.21(82)	0.68(1.5)	100.74(22)	0.81				
CPX	4.11(38)	0.51(10)	100.01(23)	0.89				
R389								
Liq	8.05(12)	0.14(3.7)	94.02(25)	0.76		6	0.15	100.18
Ol	10.91(82)	0.06(31)	99.88(31)	0.89	0.40			
Gt	8.01(59)	1.23(1.6)	99.84(18)	0.81				
CPX	4.41(32)	0.49(0.9)	99.63(14)	0.88				
R398								
Liq	8.56(12)	0.12(12)	94.23(83)	0.75		5.41	0.38	100.03
Ol	9.51(26)	0.06(11)	100.54(45)	0.90	0.33			
Gt	8.24(23)	0.64(0.9)	100.83(107)	0.82				
CPX	4.31(12)	0.34(1.5)	100.27(59)	0.89				
R396								
Liq	8.66(16)	0.09(10)	93.07(34)	0.74		4.78	0.33	98.18
Ol	10.78(52)	0.03(0.8)	100.02(10)	0.89	0.36			
Gt	8.13(17)	0.80(15)	101.00(22)	0.82				
CPX	4.60(11)	0.43(1.3)	100.38(60)	0.88				

R380IC								
IC Liq	11.5(32)	0.15(1.6)	94.13(54)	0.71		2.7	0.24	97.08
IC OL	12.76(81)	0.06(20)	100.17(37)	0.87	0.36			
IC GT	9.48(22)	0.60(1.8)	99.64(41)	0.78				
R380OC								
Liq	9.44(27)	0.11(0.7)	94.46(52)	0.73		4	0.61	99.07
Ol	10.40(48)	0.04(23)	99.82(31)	0.89	0.33			
Gt	7.69(21)	0.67(9.7)	99.41(45)	0.82				
CPX	4.37(18)	0.49(1.4)	99.48(52)	0.88				
R393 IC								
Liq	11.30(17)	0.15(2.1)	92.68(47)	0.68		4.1	0.08	96.86
Ol	12.95(48)	0.07(24)	100.66(37)	0.87	0.33			
Gt	8.70(34)	1.05(3.2)	100.25(56)	0.80				
R393OC								
Liq	8.58(13)	0.10(2.8)	93.39(22)	0.74		4.1	0.105	97.60
Ol	10.76(14)	0.03(0.6)	100.65(24)	0.89	0.36			
Gt	7.85(38)	0.60(14)	100.00(16)	0.82				
CPX	4.18(15)	0.31(8.1)	99.82(18)	0.89				

Table 2: Full experimental results, concentrations given in weight percent. 2 samples do not have cpx analyses presented; the cpx grains available were small and we were unable to obtain electron probe analyses that were not contaminated by the exterior quench layer. An average of these liquid compositions was used to calculate the final representative liquid given in Table 3, with edits to the TiO_2 concentration as discussed in the text. Values in parentheses are 100 * the standard deviation of the electron microprobe measurements. Errors on volatile contents are ~10% relative, as discussed in the text.

Table 3

	This work					
	Hydrous	Volatile-free	pHMELTS	Longhi	Walter	Gaetani and Grove
SiO_2	44.56	47.42	42.44	45.60	46.17	43.88
Al_2O_3	12.60	13.41	8.97	15.10	13.32	15.41
CaO	9.40	10.01	3.00	6.91	10.69	10.2
MgO	14.01	14.91	15.58	15.30	16.90	13.36
FeO	9.04	9.62	9.59	9.60	9.55	8.21
Na_2O	2.78	2.96	15.03	2.68	0.96	2.2
K_2O	0.38	0.41	0.00	2.13	0.56	0.1
MnO	0.15	0.12	0.00	0.21	0.18	0.12
TiO_2	0.90	0.96	1.16	1.43	0.91	0.64
Cr_2O_3	0.12	0.12	1.61	0.22	0.31	0.15
H_2O	4.95		2.56			5.3
CO_3	0.10					1.25

Table 3: Our given liquid composition estimated to be an average hydrous liquid that could be produced by melting KLB-1 under the pressure and temperature conditions used here. The composition is presented on a hydrous basis and renormalized to a volatile-free basis to allow for comparison between studies. The pHMelts liquid was calculated as described in the text. The liquid from Longhi (2002) is their calculated 1% melt of PUM. The liquid from Walter (1998) is experiment 30.12, which is the lowest temperature liquid

composition given from 3 GPa, although the solid assemblage for this sample did not include garnet. The liquid from Gaetani and Grove (1998) is sample B365. These liquids (all normalized to volatile-free conditions) are plotted in figure 7.

FIGURE CAPTIONS

Figure 1: Backscattered electron image of a section of a typical recrystallized peridotite. High relief, bright grains are garnet, lower relief or small grains are cpx, and the darker matrix is composed of olivine grains. Typical grain size is ~20 μm for the garnets and the olivines and ~10 μm for the cpx. Voids are formed where grains were plucked during polishing. Bright spot is a surface contaminant.

Figure 2: Schematic capsule design. Outer capsule and inner capsule are loaded with identical glass starting material, with additional solid peridotite added to inner capsule. Inner capsule is an Fe-preconditioned Au_{75}-Pd_{25} metal, outer capsule is made of Fe-preconditioned Pt.

Figure 3: Backscattered Electron Images of experimental run products. (a) The melt pool at the top of R380. Some quench needles can be seen at the bottom of the image, along with several spots showing polishing or probe-beam damage. AuPd capsule is pure white in this image. (b) The solid pile from the bottom of the same run. Dark crystals are olivine grains, lighter crystals are garnet and cpx. Bright rims around most grains are quench features. Dark, interstitial material is composed of glass or partially crystalline groundmass that has lost much of its MgO, FeO, and often CaO to the quench boundaries on the grains. Horizontal elongate features are cracks formed on quench; occasionally they appear to have bright spots due to polishing material or epoxy being trapped within them. Circular features in Figure 3a also appear to be related to polishing damage or

plucking; they were polished to variable depths and confirmed not to be vesicles optically.

Figure 4: Measured volatile contents for these experiments compared with the volatile contents of Gaetani and Grove (1998) (red point) and the field of volatile contents (blue ellipse) from the experiments of Liu et al. (2006). Our experiments are not only at higher pressure than previously conducted experiments, but they also sample a range of volatile contents that has not been sampled previously.

Figure 5: Example FTIR spectra of glasses. (a) 3600 cm^{-1} water peak from sample R393, thinned down to ~45 μm to bring this peak on scale. (b) The characteristic structure seen in our OH^- peak spectra. The peak near 4000 cm^{-1} is typical of water-bearing glasses, but the peak at 4500 cm^{-1} is split into multiple peaks. Calculating a total OH^- content using the most intense of these peaks in this range, an H_2O content using the 5200 cm^{-1} peak, and using the calibration of Ohlhorst et al. (2000), gives water contents that are indistinguishable from those measured using the 3600 cm^{-1} peak and the calibration of Dixon et al. (1995).

Figure 6: Correlation between OH^- contents and carbonate contents as measured by FTIR. Error bars are as discussed in the text. R380 (red point) falls off the trend as it is the lowest total water content sample and likely has not saturated fully in OH^-.

Figure 7: Concentration in given liquids normalized to concentration in N-MORB of Hofmann (1988). K_2O, MnO, and Cr_2O_3 were compared to a value of 0.1, as they are either not given or are impractically low in that work. pHMelts cannot include MnO or K_2O effectively, so those two oxides were not included in the calculation and their values are not plotted.

Figure 8: Molar (MgO + FeO)/SiO_2 ratios, as described in the text. Also shown in addition to our data are all data points from 3-4 GPa from Walter (1998), the two points from 2 GPa from Gaetani and Grove (1998), and the 1% melt of primitive upper mantle (PUM) at 3 GPa from Longhi (2002). Increasing water in our samples and those of Gaetani and Grove (1998) is associated with increasing X_{SiO2} and a decrease in the ratio $(X_{FeO} + X_{MgO})/X_{SiO2}$, and thus moves towards the lower right in this diagram. Increasing temperature and increasing degree of melting has the opposite effect and moves liquids towards the upper left. Increasing carbon content may counteract some of the effect of water, and thus the samples from Gaetani and Grove plot closer to our field from higher temperature and pressure than might be expected at lower carbon contents. The calculated melt from pHMELTS is also shown. Figure 8b shows the correlation in our samples between increasing water content and decreasing $(X_{FeO} + X_{MgO})/X_{SiO2}$.

Figure 9: Solid and liquid compositions from the experiments presented here plotted in the model system olivine/nepheline-calcium aluminate/larnite/quartz, as described by Longhi (2002). Abbreviations: Jd/CaTS (jadeite/calcium-tschermakite), AnAb

(anorthite/albite), Gt (garnet), OPX (orthopyroxene), Di (diopside), Qtz (quartz), Ol (olivine), NeCa (nepheline-calcium aluminate), Wo (wollastonite) and CPX (clinopyroxene). Here the compositions are projected from wollastonite onto the Ol-Qtz-NeCA plane. Also shown are: the compositions of garnet and cpx from our anhydrous recrystallization experiments (black diamonds, labeled with arrows) and the composition of an anhydrous 1% melt of PUM calculated by Longhi (2002). Each experiment that produced measurements of a liquid, cpx, and garnet composition gives three composition points, shown connected by a triangle. In general, the points move away from the point PUM and away from olivine with increasing total H_2O plus alkali contents, as represented by the arrow. R390 (green triangles) is a notable outlier to this trend. Inset shows the full compositional triangle with the red box delimiting the area seen in the larger image.

Figure 10: Solid and liquid compositions plotted in the same normative component space as Figure 9, but here projected from olivine into the plane OPX-Wo-Jd/CaTS. Also shown are: the composition of our dry cpx and garnet (black diamonds, labeled) the composition of KLB-1 as measured by Davis et al. (2009), the fields of cpx (green ellipse) and garnet (red circle) compositions from the 2.8 GPa experiments of Longhi (2002), the edge of the cpx field at 2.8 GPa from Longhi (2002) (solid green line) the boundary of the cpx field at 0.1 MPa from Longhi (2002) (dashed green line), and the approximate position of the garnet-cpx-olivine cotectic from 2.8 GPa from Longhi (2002) (dashed orange line). Our hydrous experiments produced garnets with slightly more aluminous compositions but still within the field sampled by Longhi (2002). Our

subsolidus cpx composition falls within error on the line forming the edge of the 2.8 GPa cpx field. All of the cpx from our wet experiments shift significantly in composition towards diopside and away from albite-anorthite. This shift consists of a change in composition towards lower Al_2O_3 and higher CaO contents in the hydrous experiments. In general, increasing liquid contents of alkalis + H_2O tends to shift the liquid and cpx composition as shown by the arrows; the cpx moves away from OPX while the liquid moves towards it. Our liquids project within error on the 2.8 GPa olivine-cpx-garnet cotectic from Longhi (2002).

FIGURES

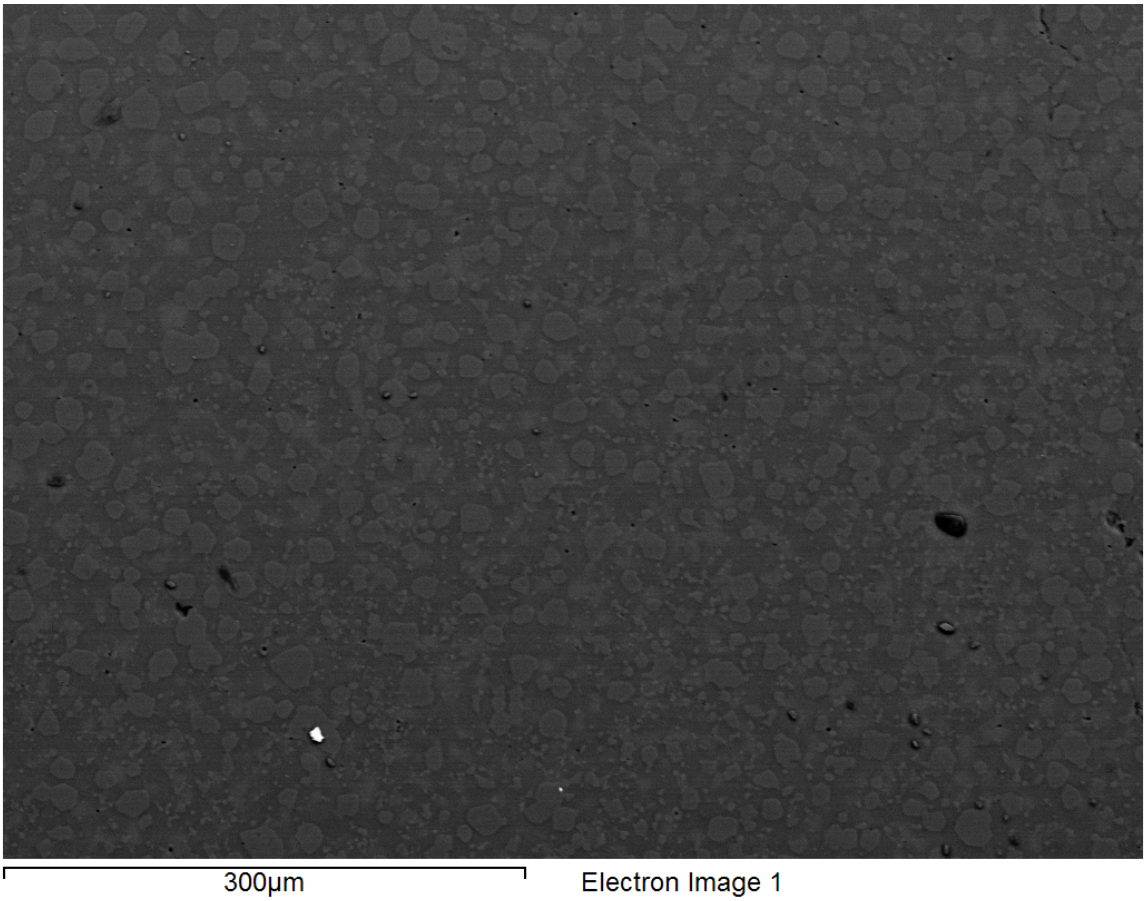

Figure 1

Figure 2

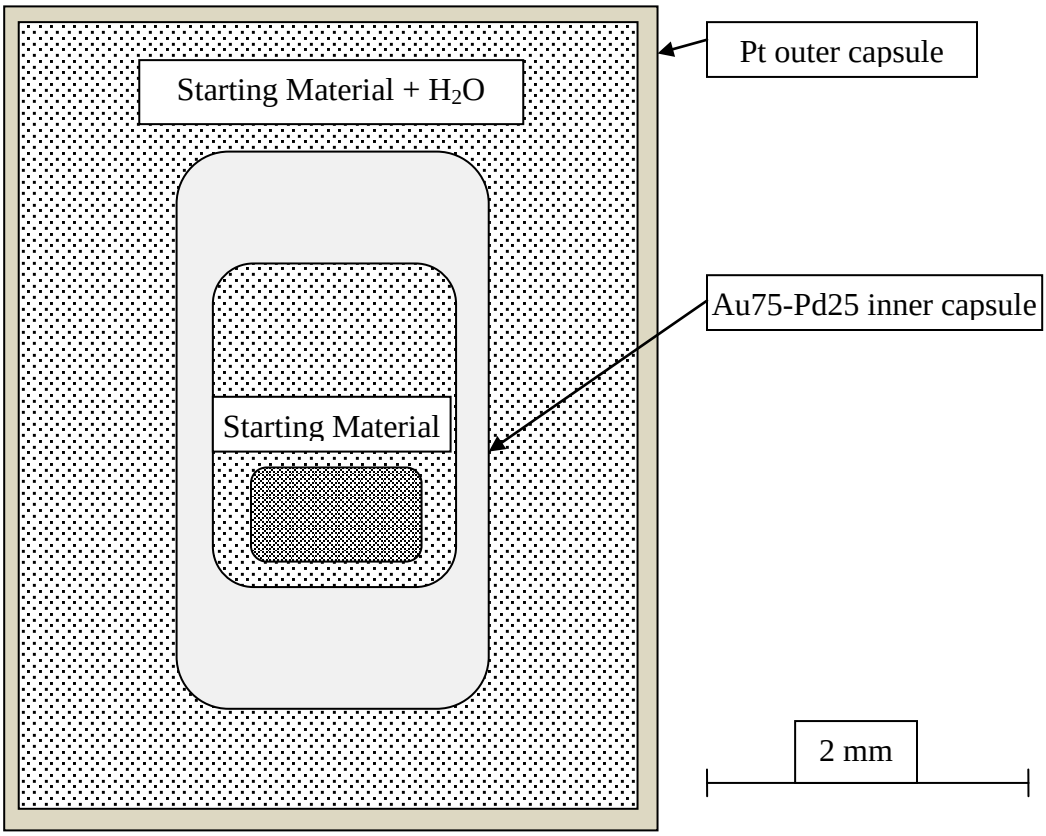
Pt outer capsule
Starting Material + H_2O
Au75-Pd25 inner capsule
Starting Material
2 mm

Figure 3

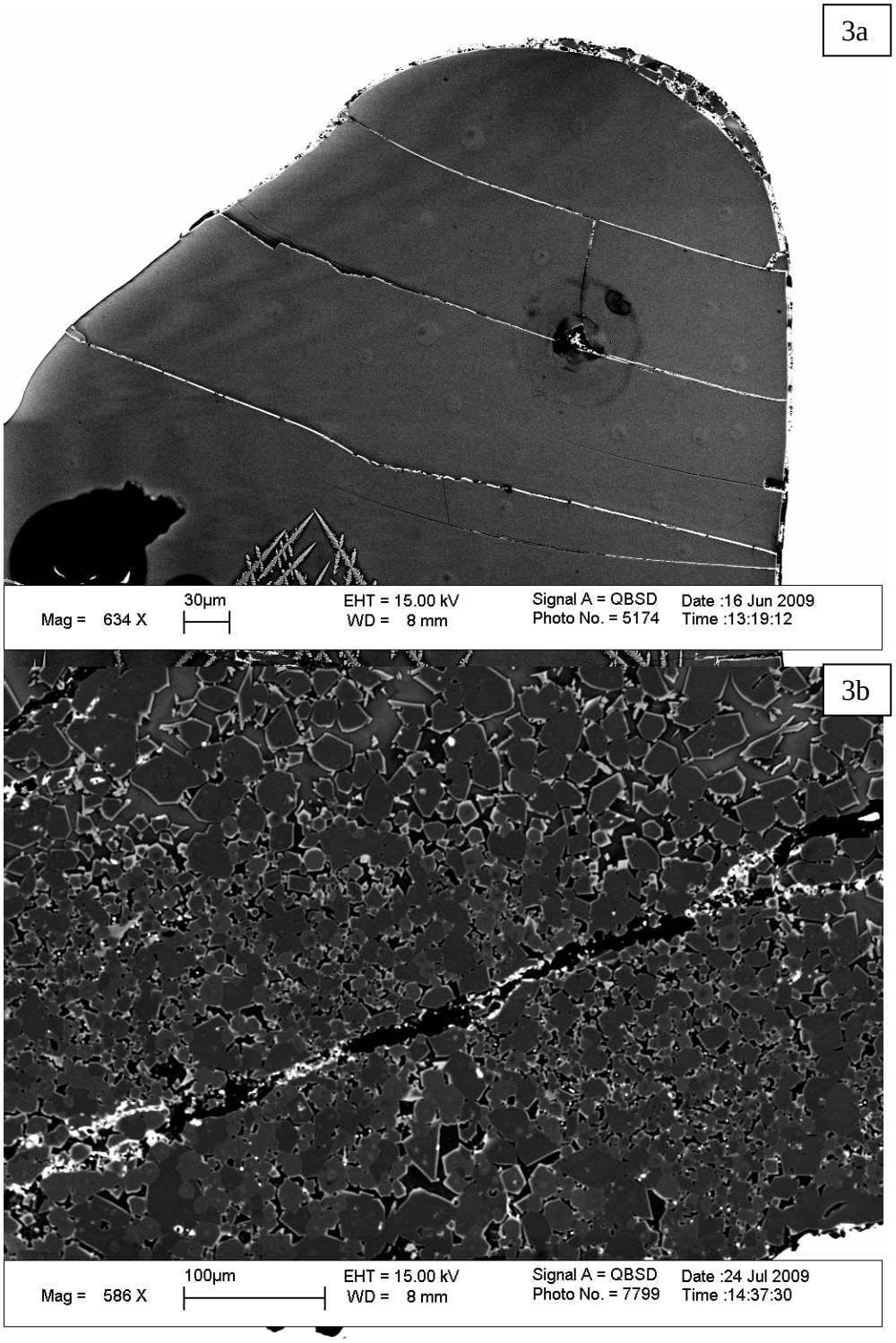
3a
Mag = 634 X
30µm
EHT = 15.00 kV
WD = 8 mm
Signal A = QBSD
Photo No. = 5174
Date :16 Jun 2009
Time :13:19:12
3b
Mag = 586 X
100µm
EHT = 15.00 kV
WD = 8 mm
Signal A = QBSD
Photo No. = 7799
Date :24 Jul 2009
Time :14:37:30

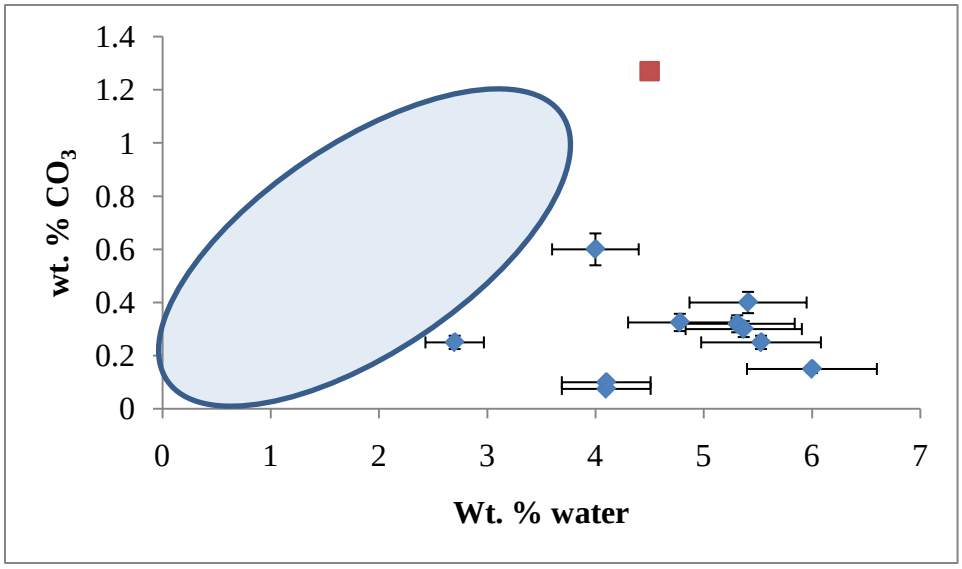

Figure 4

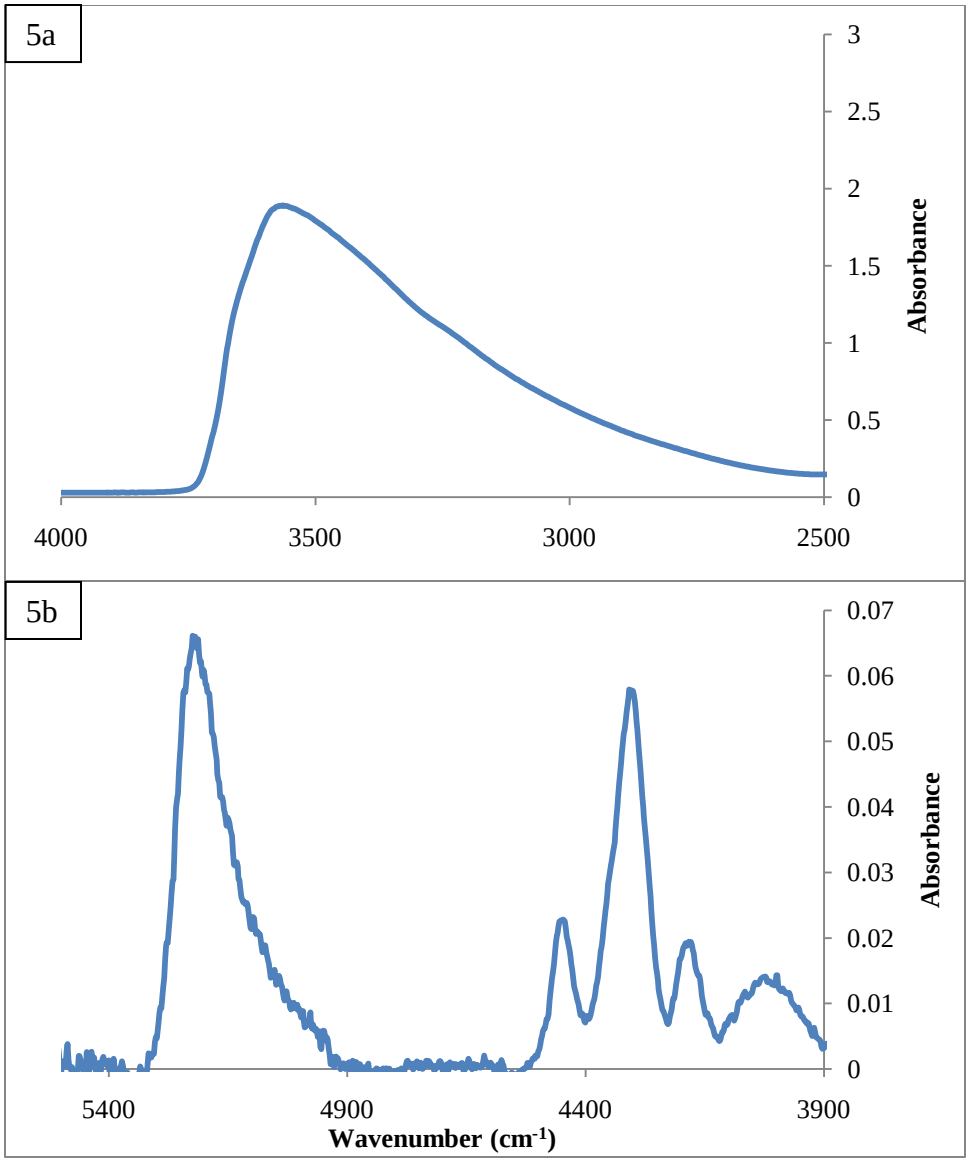
5a
3
2.5
2
1.5
1
0.5
0
Absorbance
4000
3500
3000
2500
5b
0.07
0.06
0.05
0.04
0.03
0.02
0.01
0
Absorbance
5400
4900
4400
3900
Wavenumber (cm-1)

Figure 5

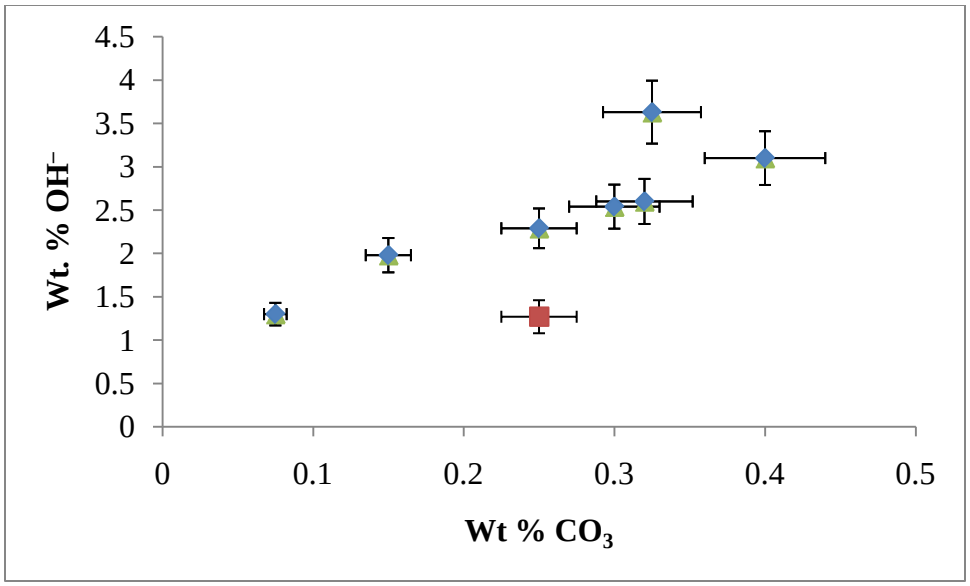

Figure 6

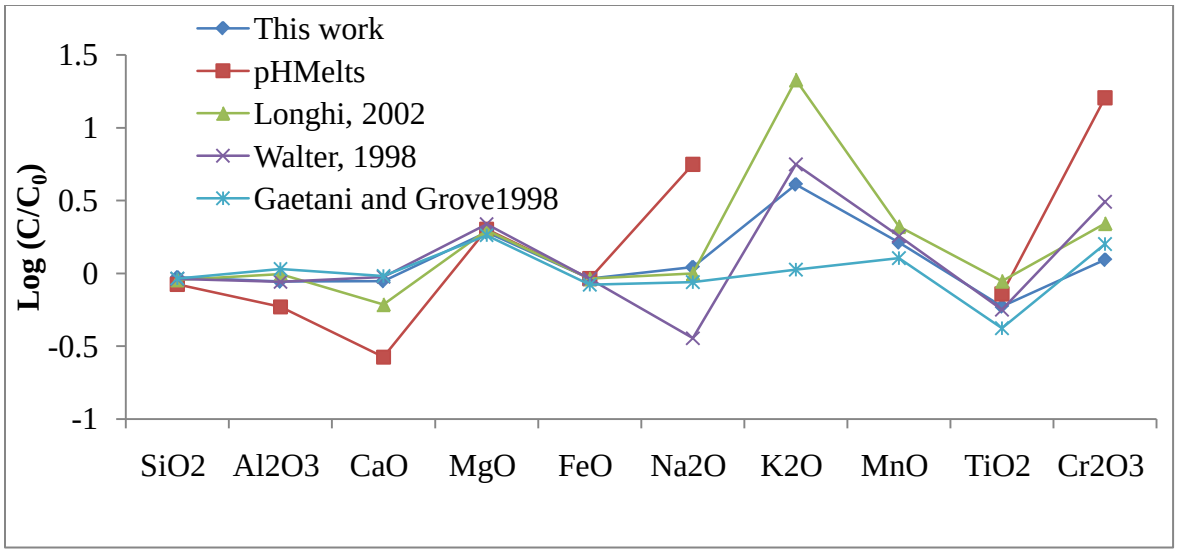
This work
pHMelts
Longhi, 2002
Walter, 1998
Gaetani and Grove1998
1.5
1
0.5
0
-0.5
-1
Log (C/C0)
SiO2
Al2O3
CaO
MgO
FeO
Na2O
K2O
MnO
TiO2
Cr2O3

Figure 7

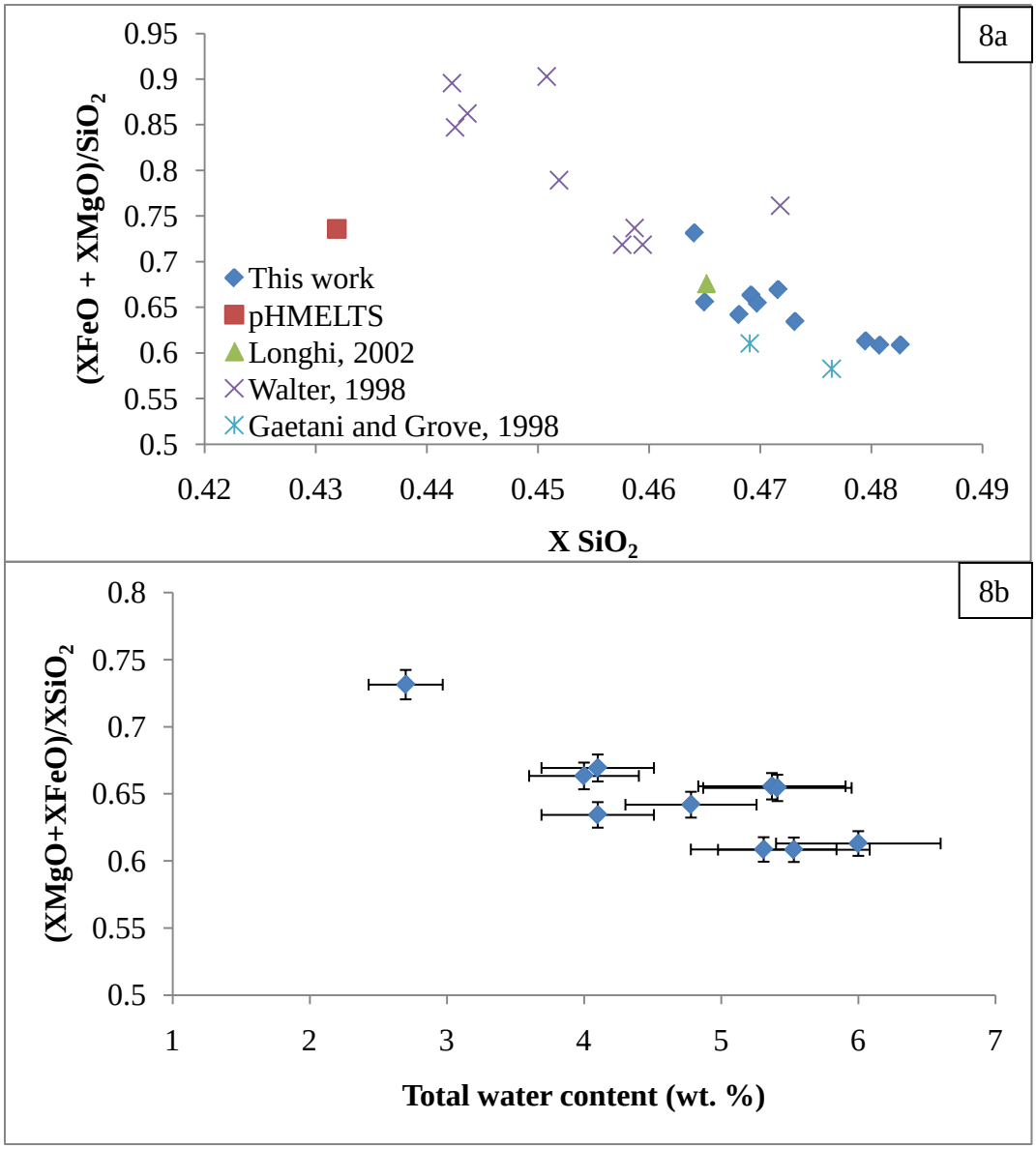
8a
0.95
0.9
0.85
0.8
0.75
0.7
0.65
0.6
0.55
0.5
(XFeO + XMgO)/SiO2
This work
pHMELTS
Longhi, 2002
Walter, 1998
Gaetani and Grove, 1998
0.42
0.43
0.44
0.45
0.46
0.47
0.48
0.49
X SiO2
8b
0.8
0.75
0.7
0.65
0.6
0.55
0.5
(XMgO+XFeO)/XSiO2
1
2
3
4
5
6
7
Total water content (wt. %)

Figure 8

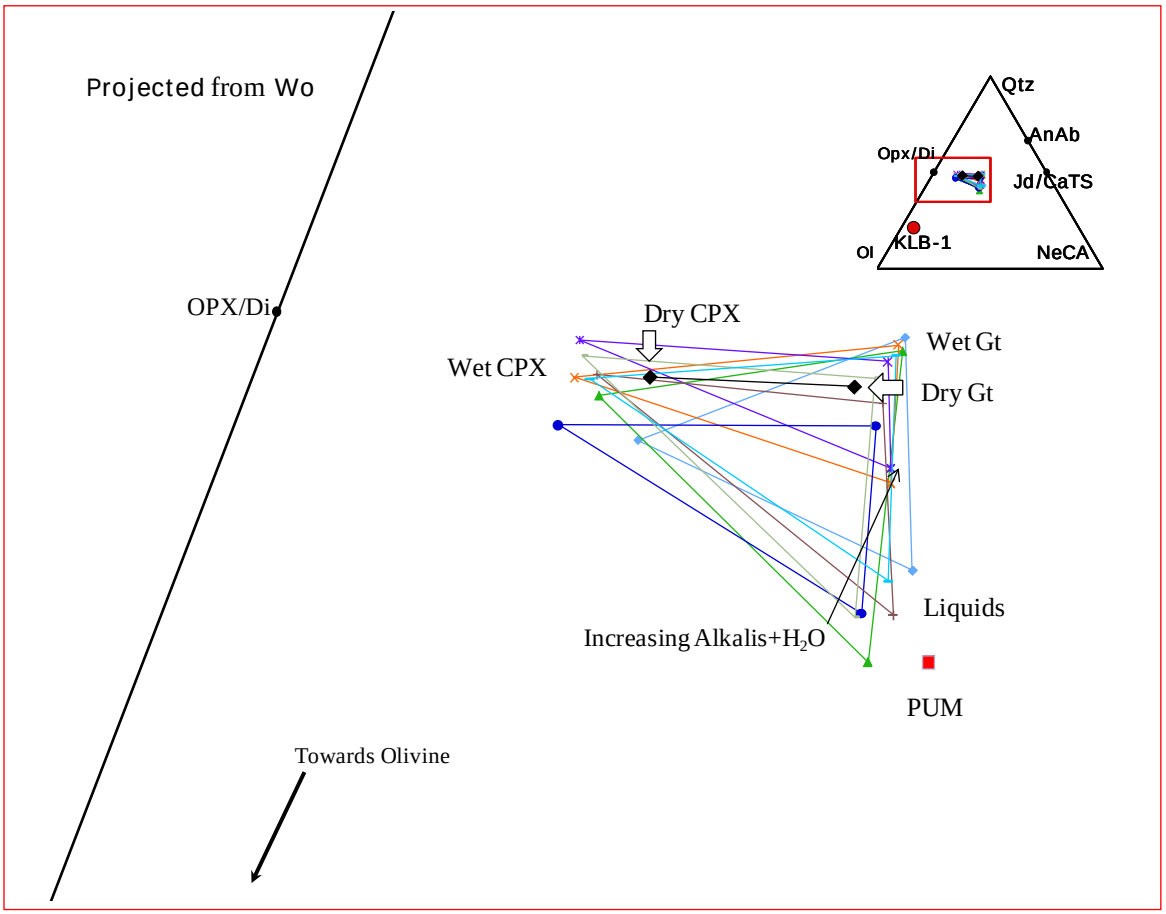
Projected from Wo
OPX/Di
Towards Olivine
Qtz
AnAb
Opx/Di
Jd/CaTS
Ol
KLB-1
NeCA
Dry CPX
Wet CPX
Wet Gt
Dry Gt
Liquids
Increasing Alkalis+H2O
PUM

Figure 9

Figure 10

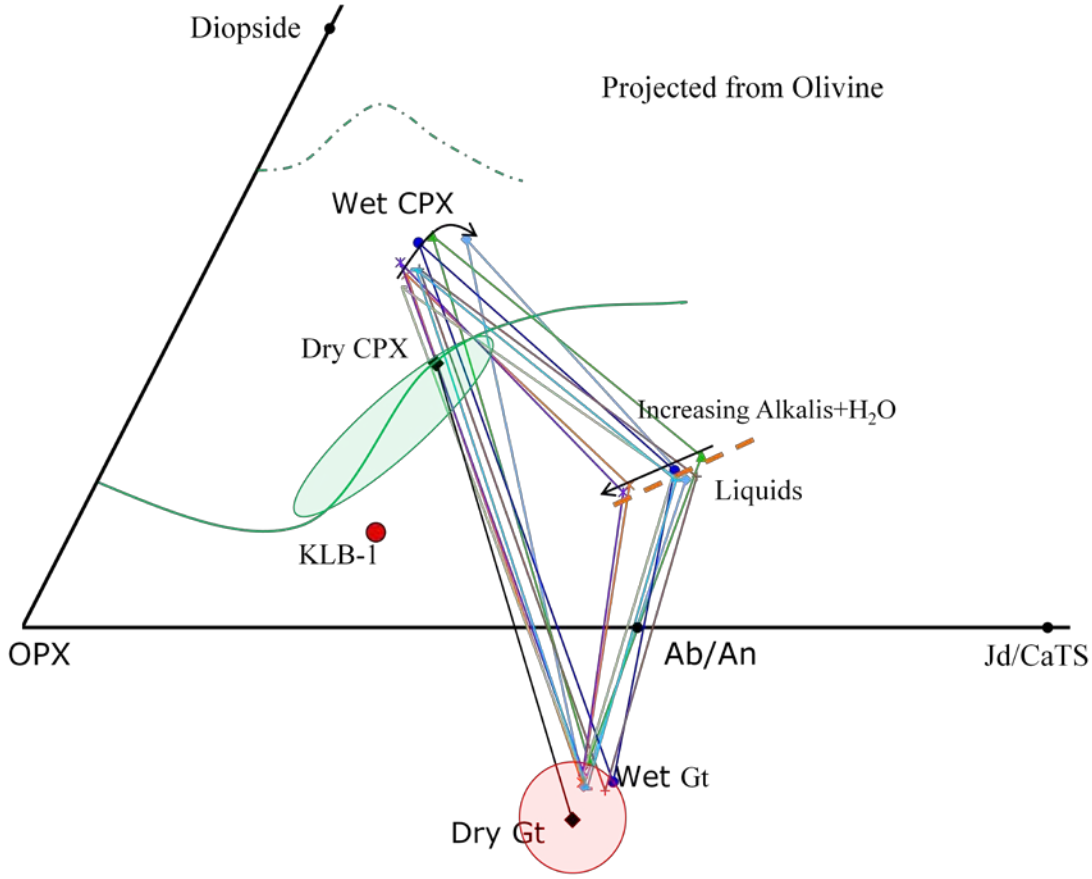
Diopside
Projected from Olivine
Wet CPX
Dry CPX
Increasing Alkalis+H_2O
Liquids
KLB-1
OPX
Ab/An
Jd/CaTS
Wet Gt
Dry Gt